

TITLE:

*MIDDLE TO LATE PLEISTOCENE PALAEOCEANOGRAPHY INFERRED
FROM RIDGE-FURROW STRUCTURES ON THE CONTINENTAL SLOPE
OFFSHORE ANGOLA*

Hugo Putuhena^{1*}

Andrew M. W. Newton²

Joe Cartwright³

Mads Huuse¹

Manuscript submitted to:

Marine Geology – special issue

* hugo.putuhena@manchester.ac.uk / samudraputuhena@gmail.com

1) *Department of Earth and Environmental Sciences, The University of Manchester, M13 9PL,
Manchester, United Kingdom*

2) *School of Natural and Built Environment, Queen's University Belfast, BT7 1NN, Belfast,
United Kingdom*

3) *Department of Earth Sciences, University of Oxford, OX1 3AN, Oxford, United Kingdom*

ABSTRACT

3D seismic reflection data have been used to map 784 enigmatic ridge-furrow structures in water depths of 0.8-1.7 km offshore Angola. The structures are characterised by asymmetric ridges with intervening furrows, typically <0.5-5.5 km long, with a sinuous to bifurcating planform. The furrows are well-imaged on seismic profiles, and range from 60-80 m in width, up to 10 m in amplitude, and 0.1-1 km in wavelength. The furrow sets aggrade in a downslope direction and occur in arrays that have an internally consistent direction that is either parallel, or slightly diverging or converging. Two alternative origins are considered: (1) furrows that are dominantly erosional scours formed from seafloor-incising currents flowing parallel to the furrows, with the ridges a by-product of the erosion, or (2) the ridge-furrows are bottom-current generated dune-type sediment waves. The latter interpretation allows us to reconstruct a key component of the deepwater bottom-currents regime along this continental margin from the Middle Pleistocene to the present-day. The most likely transport agent responsible for the interpreted sediment waves is a palaeo-bottom-current regime with a flow direction toward the west-southwest/south-southwest, the same direction of the sediment wave migration. The palaeo-bottom currents would then be expected to have a very specific flow regime with $1 < Fr_{\max} < 2$ and may originate from longshore currents cascading off the shelf, Congo Canyon distal overflows, breaking internal waves or a mixture of these processes.

1. INTRODUCTION

Seismic stratigraphic analysis can provide excellent constraints on the bottom-current behaviour across a diverse range of continental margins through the identification of bottom-current controlled depositional systems (e.g., Gruetzner et al., 2014; Hohbein and Cartwright, 2006; Lamb et al., 2017; Miramontes et al., 2020, 2021; Palanques et al., 2006). Advances in seismic reflection imaging and the wider availability of 3D data, have led to refinements in the seismic stratigraphy of bottom-current controlled depositional systems and allow for the direct observation of their bedforms and evolution through time (Faugères et al., 1999; Hernández-Molina et al., 2016; Rebesco et al., 2014). The seismic geomorphology of these bedforms can also help us to better understand the relationship between bottom-currents and sedimentary processes – e.g., how bottom-current flow direction and strength influences bedform morphology and grain-size distribution (McCave, 1971; Stow et al., 2009).

Linear erosive furrows and moats are a typical seismic geomorphological expression of contourites and their presence has frequently been used to unravel palaeoceanographic conditions across a diverse range of environmental and geological settings (e.g., Hernández-Molina et al., 2006; Lamb et al., 2017; Lobo et al., 2011; Nugraha et al., 2019). Although the term ‘furrow’ has been used in other studies to describe linear erosive features formed by iceberg/stumoki scouring or linear depressions considered as non-erosive features (Table 1) (e.g., Gay et al., 2004; Halberstadt et al., 2016; Newton et al., 2016, 2018).

In this study, hundreds of furrow structures with intervening ridges have been mapped using 3D seismic reflection data from the continental slope of the Lower Congo Basin, offshore Angola (Fig. 1). Previously, the presence of furrows with a similar character were recognised in a 3D seismic survey located to the north of the Congo Canyon (Gay et al., 2004). Furrows with a similar seismic expression can also be observed on data published from elsewhere along the West African passive margin (e.g., Lonergan et al., 2013, Maia et al., 2016, Serié et al., 2017), even though they were not described specifically in those studies (Fig. 1 and Table 2). The main aims of this paper are to provide a rigorous description of the ridge-furrow arrays in the study area using 3D seismic data, place this descriptive framework into a regional

context, and from this infer the origins of the ridge-furrows and their palaeoceanographic significance.

2. STUDY AREA

2.1. Oceanographic background

The 3D seismic reflection data used in this study are located on the continental slope of the Lower Congo Basin in the eastern South Atlantic Ocean, in water depths of 0.8-1.7 km (Fig.1,2). The upper layer of the water-column in the region is filled with surface water (SW) that is circulated by the Angola Currents (AC) or Benguela Coastal Currents (BCC) (Hardman-Mountford et al., 2003; Hopkins et al., 2013) and Congo River discharge (Fig.2). The SW that is carried by the AC is characterised as a fast, narrow, stable, warm, and saline water mass that occupies a water depth range of 0-300 m (Table.3) (Jatiaux et al., 2017, 2018; Hardman-Mountford et al., 2003). While the SW carried by the BCC is characterised as cold with a lower salinity but with a similar velocity to the AC (Table.3) (Jatiaux et al., 2017, 2018; Hopkins et al., 2013). The SW carried by the BCC is commonly located on the surface or beneath water carried by the AC (Jatiaux et al., 2017, 2018). The Congo River discharge has a similar velocity magnitude, but warmer and less saline water than the SW, while it disperses in a basinward direction in water depths 0-20 m (Jatiaux et al., 2017, 2018). The mid to bottom layer of the water column in the region is dominated by the Atlantic Intermediate Water (AAIW) (at water depths 400-1200 m) and North Atlantic Deep Water (NADW) (at water depths 1700-2000 m), with a thin layer of upper Circumpolar Water (uCPW) between them (at water depths 1200-1500 m), which all are circulated by southward currents (Fig.2, Table.3) (Arhan et al., 2003; Stramma and Schott, 1999; Jatiaux et al., 2017). The AAIW and uCPW are circulated southward by the South Intermediate Counter Current (SICC) (Stramma and England, 1999; Stramma and Schott, 1999), while the NADW is circulated southward by the Deep Western Boundary Current (DWBC) (Jatiaux et al., 2018; Garzoli et al., 2015). Those circulating water masses are characterised as sluggish and cold with a maximum velocity magnitude <20 cm/s (Table.3) (Jatiaux et al. 2017, 2018).

Recent measurements and numerical model observations show that in general the bottom-current regime in the regional study area are shaped by longshore currents that periodically shift between southward and northward flow directions across biweekly, seasonal, and interannual timeframes (Arhan et al., 2003; Guiavarc'h, 2008, 2009; Jatiault et al., 2018; Stramma et al., 2003; Vangrieshiem et al., 2005). The biweekly shifting is influenced by the propagating deep Yanai waves formed by the remote equatorial winds (Guiavarc'h, 2008, 2009; Vangrieshiem et al., 2005). The seasonal and interannual variations are influenced by variations in solar radiation, Atlantic El Niño conditions and anthropogenic aerosol activity (Svendsen et al., 2014; Tokinaga and Xie 2011; Xie and Carton, 2004). Despite shifting directions, the bottom-current regime in the region is generally recognised to flow along the margin towards the south/southeast and is guided by the seafloor topography (Arhan et al., 2003; Garzoli et al., 2015; Jatiault et al., 2018). The domination of the southeastward flow is from the AAIW and NADW components of the thermohaline circulation driven by the SICC (Fig.2) (e.g., Arhan et al., 2003; Garzoli et al., 2015; Jatiault et al., 2018).

In the study area investigated here, two mooring stations were previously deployed to capture the current profile through the water column (Jatiault et al., 2018) (Fig.1a). Mooring station [1] was deployed from January-July 2009 and due to the short duration did not capture the full seasonal variation of the bottom-current regime. Mooring station [2] collected data from September 1997 to October 1998, including bottom-current measurements in water depths of 1200-1400 m, and these data document currents that flowed toward both the northwest and southeast. The bottom-currents profile in mooring station [2] exhibits the oscillating currents of the propagating deep oceanic waves on the slope and the high influence of the southward NADW flow as shown by how the southeastward component dominates the profile (Jatiault et al., 2018).

During the Middle Pleistocene Transition (MPT) (~1.2-0.8 Ma), the ocean thermohaline circulation underwent a major disruption marking the beginning of the 100 kyr glacial periods (Bell et al., 2015; Pena and Goldstein, 2014). This major disruption caused the south/southward flow of NADW components in the eastern part of South Atlantic Ocean, that

was dominant before the MPT, to be weakened during the period between Marine isotope stages (MIS) 25 and 21 (~950 to 860 ka) (Bell et al., 2015; Pena and Goldstein, 2014; Venz and Hodell, 2002). This weakening of the south/southeastward NADW flow was also accompanied by the stronger influence of the northward flowing Circumpolar Deep Water (CDW) south of the Walvis Ridge (Bell et al., 2015; Pena and Goldstein, 2014; Venz and Hodell, 2002). The major disruption of the ocean thermohaline circulation subsequently generated the stabilisation in the 100 kyr glacial period, by helping to facilitate the drawdown of atmospheric CO₂ and the growth of high-latitude ice sheets (Pena and Goldstein, 2014). After the major disruption, the weakening of the ocean thermohaline circulation was constrained to the prolonged glacials in the following 100 kyr glacial periods (Bell et al., 2015; Pena and Goldstein, 2014).

2.2. Geological background

The Lower Congo Basin was formed by the Gondwana breakup and rifting of the South Atlantic Ocean during the Late Jurassic-Early Cretaceous (Brice et al., 1982; Uchupi, 1992; Valle et al., 2001). Rift-controlled lacustrine basins preceded restricted marine conditions in the Aptian (125-113 Ma) that allowed the deposition of a thick (>1 km) salt layer followed by deposition of predominantly carbonates during the Albian, marls and clays from the Albian to Late Cretaceous and predominantly siliciclastic from the Late Cretaceous to Eocene (Brice et al., 1982; Karner et al., 1997; Marton et al., 2000; Schollnberger, 2001). The Aptian Salt subsequently facilitated the gravity sliding of the post-salt succession, with the gravity sliding exerting a first-order control on the geometry of the post-rift succession (Fort et al., 2004; Karner et al., 1997; Vallet et al., 2001). Based on the salt tectonic distribution, the Lower Congo Basin area is divided into three salt domains, a compressional domain characterised by abundant shallow salt structures, a translational domain characterised by the raft-graben province, and a translational domain in between (Marton et al., 2000; Tari et al., 2003). The study site is located in the translational domain.

The post-salt interval of the Lower Congo Basin sedimentation is characterised by an Oligocene unconformity separating the greenhouse period (during Late Cretaceous to early Oligocene) with low-amplitude and high-frequency sea-level alterations, and the icehouse period (during early Oligocene to Holocene) with high amplitude and frequency sea-level alterations (Bartek et al., 1991; Séranne, 1999). The oceanic and climatic changes and the beginning of African margin uplift in the early Oligocene triggered a general depositional switch from aggradation to westward progradation of the terrigenous wedge, shelf erosion, and growth of the Congo Fan system in the abyssal plain (Anka et al., 2009; Séranne et al., 1992). In the early Miocene, the increased sediment supply, in conjunction with the continuous African margin uplift and mobilisation of the salt, modified the turbidite deposition across the shelf and upper slope of the basin (Anka et al., 2009; Broucke et al., 2004; Oluboyo et al., 2014). After the Miocene, the acceleration on the margin uplift-rate and the instability of rising diapirs resulted in deeper incision and northwestward shift of the Congo Fan. This left the coarse-grained sediment supply along the shelf and slope to be contained inside the canyon and fine-grained hemipelagic sediments to be deposited elsewhere (Anderson et al., 2000; Anka et al., 2009; Berger et al., 1998; Broucke et al., 2004).

The early Pliocene-Recent interval is dominated by clays with a biogenic fraction of diatom and nannofossil ooze (Bolli et al., 1978; Berger et al., 1998; Pufahl et al., 1998). This interval is also characterised by a regionally extensive polygonal fault system (PFS) within the Pliocene to Pleistocene sediments (e.g., Andresen and Huuse, 2011; Gay et al., 2004; Maia et al., 2016). The genesis of polygonal faults has been widely debated with recent experimental work suggesting the diagenesis of fine-grained sediments or shear failure under low confining stresses as the most likely candidate (Cartwright, 2011; Shin et al., 2008). Gay et al. (2007) argued that the polygonal faults may act as direct conduits for fluid migration in the shallow interval, which was challenged by Maia et al. (2016) since they found that polygonal faults system may not directly act as the conduit but instead control the formation of pipes structures that actually act as the direct conduits.

2.2.1. The Congo Fan system

The Congo Fan system is located ~150 km north of the study site (Fig.1) and is among the largest active turbidite-systems that directly transports mud-rich sediments into the deep-sea (Droz et al., 2003). The formation of the recent Congo Fan architecture was initiated in the Miocene-Pliocene transition at ~5 Ma as the result of the interaction between the erosion linked to an accelerated margin uplift and the instability created by the structural growth of rising diapirs on the salt ridge (Anka et al., 2009). The total area covered by the fan is up to 330000 km², with 21400 km² of it covered by the canyon and deep-sea channel-levee system where turbidite sedimentation is active. Abandoned channels with prevailing hemipelagic deposition covers 280,000 km² of the current areal extend (Babonneau et al., 2002; Savoye et al., 2009). The Congo Fan extends 800 km basinward from the coast, to a maximum water depth of ~5600 m.

Based on its morphology and architecture, the Congo Fan can be divided into four zones: canyon, upper-fan valley, the upper channel-levee system, and the lower channel-levee system leading to distal lobes (Babonneau et al., 2002). The canyon is located at water depths of 0-2000 m (with width up to 15 km and relief ranging from 0-1300 m), while the upper-fan valley is located at water depths of 2000-3300 m (with width ranging from 4-9 km and relief ranging from 250-900 m) and the (upper and lower) channel-levee is located in water depths of 3300-4800 m (with width ranging from 1-2 km and relief up to 250 m) (Babonneau et al., 2002). The Congo Fan has a single source point due to the landward incision of the Congo Canyon throughout the wide continental shelf (~150 km) that has caused the Congo River to directly link to the canyon, allowing a direct transfer of sediment from the river into the deep-sea (Babonneau et al., 2002; Droz et al., 2003; Savoye et al., 2009).

The Congo Canyon/Channel is characterised with a deep incision of the channel floor that is even lower than the regional seafloor along its whole path (Babonneau et al., 2002). The deep incision may due to the preservation of the equilibrium profile during the incision of the canyon (Babonneau et al., 2002). The entrenchment of the Congo Canyon/Channel limits the overflow of the turbidity currents and inhibit/prevent channel avulsion, resulting in a

maintained sediment load and turbidity flow energy (Babonneau et al., 2002, 2004). Hence the sediment load thus mainly occurs along the lower fan, to result in lengthening of the Congo Channel (Babonneau et al., 2002, 2004).

The Congo Fan has at least 100 channel-levee systems from three sub-fans: the Northern (880-540 ka), Southern (540-210 ka), and Axial Fan (210 ka-present day) (Droz et al., 2003; Marsset et al., 2009). In the present-day, only a single channel-levee is active at any given time. Over the late Quaternary, the channel-levee-lobe systems has undergone lateral architectural changes of increasing/decreasing channel lengths and basinward/landward migration of avulsion points, corresponding to prograding/retrograding architectural fan cycles (Marsset et al., 2009; Picot et al., 2016). Studies of the Axial Fan show that climatic factors controlled by the West African monsoon are the primary control of architecture and timing of avulsions of the channel-levee-lobe systems (Laurent et al., 2020; Marsset et al., 2009; Picot et al. 2016, 2019). During the humid period, the progradation system occurs with high fluvial discharge and chemical erosion, elevating the transport capacity of the turbidity currents (Marsset et al., 2009; Picot et al. 2016, 2019). During the arid periods, the retrogradation system occurs with low intensity rainfall, limited runoff, and predominance of mechanical erosion due to limited vegetation cover on land resulting in a decreased transport capacity of turbidity currents (Marsset, et al., 2009; Picot et al., 2016, 2019). During the arid/humid transition periods, retrogradation and up-fan avulsions occur from new increases in the transport capacity of turbidity currents after the onset of high precipitation and fluvial discharge (Marsset et al., 2009; Picot et al. 2016, 2019).

3. DATA AND METHODS

3.1. 3D Seismic data

The 3D seismic reflection data used in this study extend over 5000 km² of the mid-slope region of the basin (Fig. 1). Lateral resolution in the shallow interval is 25 m (twice the bin size of 12.5 m; Bacon et al., 2007), and vertical resolution is ~6 m using the quarter-wavelength criterion (dominant frequency is 65 Hz and the average seismic velocity is

estimated at 1500 m/s). The seismic display is zero phased, European standard, with blue (or white) reflections indicating negative amplitudes representing a positive acoustic impedance contrast and red (or black) reflections the opposite. Several seismic reflection surfaces were generated using Petrel and PaleoScan software packages, with each pick based on the tracking of a continuous (-) or (+) amplitude seismic reflection (e.g., Posamentier, 2004). Seismic volume attributes (amplitude, dip and variance) were extracted for each seismic horizon map to aid interpretation of subtle stratigraphic features and seismic facies distribution.

3.2. Stratigraphic framework

No well data were available in the study area, so the seismic stratigraphic interpretation is based on nearby correlations from a previous study (Andresen and Huuse, 2011), where the seismic data intersects the data used here (Fig.1). The picking of key seismic markers for this study, horizon TG, in the western sub-basin (where the western furrow field exists) is based on the seismic reflector Cirq01 described in Andresen and Huuse (2011) (or CF-A in Uenzelmann-Neben et al., 1997/base IV in Gay et al., 2004/C1 in Maia et al., 2016). This seismic marker has a continuous reflection with strong negative amplitude at the top of the polygonal faults tier that separates the units in between (Andresen and Huuse, 2011; Maia et al., 2016; Uenzelmann-Neben, et al., 1997). Different ages have been assigned to this seismic marker, from the top of the Gelasian stage (1.8 Ma), MIS 12 (440-470 ka), and end of MIS 14 (540 ka) (Gay et al., 2004; Uenzelmann-Neben, 1998; Droz et al., 2003). Here, we follow the assignment of Top Gelasian as the seismic marker age stated by Andresen and Huuse (2011), as this can be correlated within the current study site. The age determination was supported by unpublished internal industry reports. While the TG horizon in the eastern sub-basin (where the eastern furrow field exists) was linked through the 3D seismic data loop tying to the west sub-basin. The TG horizon in the eastern sub-basin has a dimmer negative reflection in the sub-basin than the western sub-basin while also topping the polygonal faults tier.

The readily identified furrow structure axes (e.g., Fig.3) were spatially mapped in ArcGIS software and used to help characterise the geometry (i.e., orientation, spacing,

sinuosity index, and bifurcation) and migration characteristics of the more subtly expressed ridge structure axes.

4. RESULTS

The ridge-furrow structures in the study area are distributed across two main regions of the slope, which are referred to as 'fields' (Fig.4). The western furrow field contains 659 distinct furrows and is located above the salt mini-basin province. The eastern furrow field contains 125 furrows and is located above the raft-graben province (Fig.4a). The ridge-furrow structures are not confined to the seabed surface as they occur throughout the shallow interval above the Cirq-1/TG surface (~Top Gelasian age/1.8 Ma – TG surface) (Fig.4b). The ridge-furrow fields occur in areas where the slope measures 0.63° to 1.37° (Fig.4a) and are gentler than in the rest of the study area. Ridge-furrows are absent from areas with shallow salt structures (as shown on Fig.4), where raft structures outcrop at the seafloor (Fig.4), and where steeper seabed slopes are present (>1.55°– Fig.4a). The ridge-furrows are also locally absent from areas with pronounced clustering of seabed pockmarks linked to pipe-structures around salt diapirs (Andresen et al. 2011) (Fig.5). A Plio-Pleistocene PFS is observed beneath areas with and without ridge-furrows in the overlying stratigraphy (Fig.5).

4.1. Ridge-furrow geometries

On the seabed surface, furrow appearance has not been impacted by the underlying PFS (Fig.4a). The majority of furrows in both fields are observed to range from 0.5 to 2.5 km in length, elongated in a west-northwest–east-southeast direction (rotated 15-45° anticlockwise from the slope contours) (Fig.6). The furrows measure 60-80 m in width and are up to 10 m deep (Fig.3). The average spacing between furrows is typically 100-400 m, with a minority exceeding ~1000 m (Fig.7). The individual longitudinal geometry of most furrows is classified as almost straight with a sinuosity index (SI) generally ranging from ≥ 1.0 to 1.05, with only a few outliers of 1.05-1.25 SI (Fig.8a, 8b). Some furrows bifurcate towards their west-northwest and east-southeast ends, with up to 80 bifurcation points identified (Fig.8c, 8d). A

small subset of the total furrow population is coincident with pockmarks (13/784 or 1.7 % furrows on the seabed surface) and there does not appear to be a systematic relationship between the position of the pockmark relative to the length of the furrow.

On the TG surface, the deepest surface with ridge-furrow structures, underlying polygonal faulting has modified the geometry of the features, making it difficult to measure morphological parameters except for longitudinal axes. The dimensions of the furrow longitudinal axes are larger than the polygonal faulting, meaning their morphology is distinguishable from the polygonal faulting pattern. The longitudinal axes are recognisable in both western and eastern furrow fields, although the ridge presence is barely recognised (Fig.4b), and they display a broadly similar orientation to those on the seafloor.

In the eastern furrow field, the furrows spatial alignment displays some curvature that is convex in a southwest to south-southwest direction, in contrast to the furrows in the western furrow field that are relatively straight (Fig.9a,10a).

4.2. Ridge-furrow structures

In the shallow interval between the TG surface and seabed, furrows are observed as 'u' shaped convex downwards depressions. These are observed on continuous low-to-moderate amplitude seismic reflections that may represent fine-grained hemipelagic deposition (Fig.3b, 11a, 11c). The seismic reflection profiles show that furrow structures appear to be stacked, with the negative relief geometry of the furrow migrating in a southward direction through time (Fig.11a, 11c). The intervening ridges are subtler and can only be seen to exhibit positive relief at the present-day seabed (Fig.3b).

4.3. Ridge-furrow structures and polygonal faults

Spatial patterns derived from the furrow axes in the TG to seabed interval and the Plio-Pleistocene PFS can be observed within the 3D seismic volume (Fig.9-13). Seismic mapping demonstrates that the typical thalweg of the furrows is orientated in a west-northwest–east-southeast direction and crosscuts the omni-directional (polygonal) fault pattern beneath. Strike

orientation of the polygonal fault population has a wide scatter, with outliers (>7.5 % occurrences from the total population) that are elongated either in a west-east or northwest-southeast to north-northwest–south-southeast direction in the western furrow field (Fig.9) and either in west–east or north-northwest–south-southeast direction in eastern furrow field (Fig.10).

On seismic profiles perpendicular to the axis of the furrow the furrow stacking trajectory is more gently dipping than the relatively steep underlying polygonal faults (Fig.11a, 11c). The furrow stacking pattern dips 10° to northeast, whilst the polygonal faults pattern dips 45-60° to the horizontal surface (e.g., Fig.11a, 11c – note that these seismic cross-sections have been vertically exaggerated). It was also observed that on the seismic profiles the stacking of furrows only occasionally connects with the underlying polygonal faults that extend into the furrowed stratigraphic interval (Fig.11-a, 11-c) (cf., Fig.11-12 in Gay et al., 2004).

4.4. Furrow migration

A comparison of furrow longitudinal axes on surfaces between the TG and seabed revealed that the axes of the furrow sets migrate laterally through time in this interval (Fig.12, 13). Furrow axes can be positioned to within 25 m (the lateral resolution of the seismic data) and the gross lateral migration distances across the full span of this interval ranges from 100-400 m (Fig.6), greater than any resolution artefact. The lateral offset of furrow axes between the TG surface and the seabed indicates migration down slope, toward either the southwest or south-southwest (Fig.6, 12f, 13f).

Furrow migration (summarised on rose diagrams: grey column in Fig.6) is also evident on seismic cross-section profiles by the dip of furrow axes stacking patterns extending from those first observed on the TG surface to those on the modern seabed. Representative examples of this stacking pattern in both fields are shown in Fig.11a, 11c. The furrow depressions are easily recognised because where no furrows are present, these continuous background reflections exhibit a smooth geometry over distances of many kilometres. The furrow stacking patterns are dipping northeast (Fig.11).

5. DISCUSSION

5.1. Origin of the ridge-furrow structures

Similar ridge and furrow seismic structures were previously identified by Gay et al. (2004) to the north of the Congo Canyon on the continental slope of Lower Congo Basin. In that case the structures are spatially extensive and aggrade vertically, whereas in this study, the structures were isolated in areas with a gentle slope at certain water depths and have a clear downslope migration trend. In that study, they suggest the structures are an early development of the PFS. The basis of that interpretation is: (1) the presumption that the PFS originated by the compaction of fine-grained sediments by gravity loading in the shallow interval; (2) the perpendicular relationship between furrow orientation and the slope dip direction; (3) the apparent correspondence between furrow orientation and the dominant pattern of the underlying PFS (e.g., Fig.7-8 in Gay et al., 2004); and (4) that in seismic cross-sections the presence of seabed furrows always link with the polygonal faults that vertically extend through the whole PFS tier (e.g., Fig.9-11 in Gay et al., 2004). The last two observations were used as evidence of a connection between the furrows and the underlying PFS. However, subsequent experimental work suggests the PFS is formed due to the diagenesis of clay-rich sediments and shear failure under low confining stresses (Shin et al., 2008; Cartwright, 2011), instead of the basin scale gravity-induced shrinking previously used to interpret furrows as the early stage of the PFS (Gay et al., 2004).

The furrow axes observed in this study site are orientated oblique to the slope direction (Fig.12a, 13a). Seismic observations described here indicate that the spatial pattern of the furrow axes is distinct from the underlying PFS (e.g., rose diagrams in Fig.9, 10). Seismic cross-sections perpendicular to the axis of the furrows show the stacked furrow axes to be much less inclined than the polygonal faults. In addition, the orientation of stacked furrow axes are only occasionally coincident with the underlying vertically extensive polygonal faults (Fig.11), unlike the study published by Gay et al. (2004). The combined seismic observations

thus suggest that there is no causative link between the furrows as part of the early development of the PFS.

The lack of evidence to support that the ridge-furrow structures originated from processes similar to those associated with the underlying PFS requires alternative explanations to be considered: 1) the furrows reflect erosional scour, with the ridges a by-product of that incision (Fig.14a-b), or 2) the ridge-furrow structures represent the typical ridge-trough topography that is associated with sediment waves formed by bottom or gravity currents (Fig.14c-f).

5.2. Ridge-furrow structures and oceanographic context

5.2.1. Erosional scour as the ridge-furrow structures

Conceptually, if furrows are erosional scours the thalweg of the furrows must be parallel to the bottom-current flow direction (Hernández-Molina et al., 2008; Rebesco et al., 2014) (Fig.14a-b, 15c). The bottom-current should also be persistent, directionally stable with a helical flow pattern, and strong in magnitude, but may be periodically found with quiescence (Flood, 1983; Stow et al., 2009; Miramontes et al., 2021). The seafloor in the study area is assumed to be no coarser than fine silt, as has been recorded at the nearby ODP Leg 175/DSDP Leg 40 site (Berger et al., 1998; Bolli et al., 1978). To generate mud furrows, at least >30 cm/s magnitude of bottom-currents would be required (Stow et al., 2009). In the case of the furrows in the study area, which are elongated in a west-northwest–east-southeast direction, if these features are erosional the inducing bottom-currents should be oriented parallel to the furrows orientation (i.e., toward west-northwest or east-southeast). The Coriolis Effect will also impact the migration direction and it is envisaged that furrow migration would be to the left of the dominant flow direction in the Southern Hemisphere (cf., Flood, 1994; Lamb et al., 2017; Séranne and Nzé Abeigne, 1999). In this case, in which the furrows migrated to the south-southwest through time (Fig.6), it is inferred that the flow of the bottom-currents required to form these erosional scours would have been towards west-northwest (Fig.14a-b, 15c).

The inferred direction of flow to the west-northwest for the bottom-current (Fig.15c) is, however, conflicting with the dominant component of measured bottom-current regime in the region. Present-day bottom-current flow measurements from a 48 hr record at mooring station [1] indicates a dominant flow to the south-southwest (Fig.15f). While a one year record in mooring station [2] indicates a flow to the northwest alternating with a dominating flow to the southeast (Fig.15g) depicting the oscillating components of the local impact of propagating deep oceanic waves (see oceanography background). The west-northwest direction is instead only oblique slightly to the northward component of the oscillating currents (Fig.15), indicating a plausible product-origin relationship between the furrows, if they are erosive, and the northward component flow. However, the northward flow component, as shown in the bottom-current profile at mooring station [2], has a magnitude <20 cm/s (Jatiaux et al., 2018). The magnitudes of that flow are below the threshold required (see above) to erode the sea floor that would be no coarser than fine silt, as has been recorded at the nearby ODP/DSDP site (Berger et al., 1998; Bolli et al., 1978). A mechanism triggered by topographical effects such as contourite channel or gateway may intensify the northward component flow, to result in acceleration in that flow speed (e.g., Hernández-Molina et al., 2006; Stow et al., 2009). However, the furrow fields are in areas that relatively flat and broad without any presence of those topographical forms.

5.2.2. Sediment waves as the ridge-furrow structures

Two possible relationships may be interpreted between sediment wave orientation and flow direction, where each has different implications on the reconstruction of the flow origin (McCave, 2017; Wynn and Stow, 2002). First, if we use the relationship commonly found in sediment wave fields formed by turbidity/density flow currents (commonly heading downslope), the sediment waves would have longitudinal axes perpendicular to the current flow direction, roughly parallel to regional slope, and may also migrate upstream or downstream (Cartigny and Postma, 2017; Wynn and Stow, 2002). Second, if we use the relationship commonly found in sediment waves formed by bottom-currents, the flow direction

tends to be oblique with a steep angle ($<45^\circ$) to the wave longitudinal axes (McCave, 2017; Wynn and Stow, 2002). The sediment waves may migrate upstream (as mostly found in observations) or downstream depending on the fluid dynamics (Cartigny et al., 2011; McCave, 2017) to the left of the flow direction in the Southern hemisphere due to the Coriolis Effect (Wynn and Stow, 2002) or just aggrading without migration (McCave, 2017). These concepts of sediment wave formation, orientation and migration in relation to bottom flow direction and position on the continental slope were used to derive potential models of all plausible flow directions that may yield the observed sediment wave profile, as depicted on Fig.14b-n.

5.2.2.1. *Sediment waves originating from perpendicular flows to wave crest*

The relationship between density flow currents and sediment waves, suggest that the observed sediment waves could be formed by a flow that is perpendicular to the longitudinal axes of the crest, such as a flow toward the south-southwest (Fig.14c-d) or the north-northeast (Fig.14e-f). The flow direction in the latter scheme would, however, mean the density flow would be going slightly upslope, meaning it can be confidently discounted as a possible origin for the sediment waves. In the former scenario, a south-southwest flow direction would align with the observed wave migration direction and the sediment waves would then have a dune character (Cartigny et al., 2011), giving the inducing flow an expected Froude Number (Fr) of between 1-2 (Cartigny et al., 2011).

5.2.2.2. *Sediment waves originating from slightly oblique flows to wave crest*

Following the relationship between bottom-currents and sediment waves, it would be plausible for the observed sediment waves to be formed by bottom-currents flowing toward a range of directions: north-northwest (Fig.14g-h), west-southwest (Fig.14i-j), east-northeast (Fig.14k-l), and south-southeast (Fig.14m-n), to create an angle between flow and wave crest of $<45^\circ$. However, if the sediment waves were formed by the last two possible directions, the sediment migration would be to the right of the flow direction, opposing the conceptual criteria of bottom-currents and sediment wave relationship under the influence of the Coriolis Effect

in southern hemisphere (see above), thus these possibilities can be ruled out. If the sediment waves formed from a flow to the north-northwest (Fig.14g-h), the sediment waves would then have an antidunes characteristic, since the flow direction would oppose the sediment waves migration and hence have $Fr_{max} > 1$ (Cartigny et al., 2011). If the sediment waves formed from a flow toward the west-southwest (Fig.14i-j), the sediment waves would then have a dunes characteristic, since the flow direction would be the same as the sediment waves migration and hence have $1 < Fr_{max} < 2$ (Cartigny et al., 2011).

From the analysis shown in the last two subsections, it is either a flow to south-southwest formed from a perpendicular flow-crest relationship (Fig.14c-d) or a flow toward the north-northwest or south-southwest that would then form a steep oblique flow-crest relationship (Fig.14g-j), which would meet the requirements from the conceptual model of sediment waves formation. The concept of a north-northwest flow in forming the sediment waves is contextually difficult to support. We have considered two possible origins that may form a northward flow: i) a northwestward component of oscillating currents of propagating deep oceanic waves (see oceanographic background), or ii) a northward thermohaline current. However, postulating either would be problematic. The northward flow in the former case has been measured in the contemporary setting (mooring station-[2], Jatiault et al., 2018), however, if the former case was the origin, it is uncertain why only the northward currents would lead to sediment wave migration, but the southward component, which is similar in magnitude and tends to dominate the record, would not (Arhan et al., 2003; Jatiault et al., 2018; Vangriesheim et al., 2005). Thus, the southward component would be expected to impact sediment migration as well – e.g. the migration would be at least near to zero (net impact where migration in both directions is equal) or even the other opposite way around. The observations show the furrows migrated from TG to the seabed in a consistent direction towards the south-southeast through time.

Northward thermohaline currents have not previously been reported in the region and appear contextually unlikely to occur as that would require a northward movement of a water mass in the deep circulation through a major oceanographic reorganisation that would move

the AABW or other CDW beyond the region where it is currently constrained to water depths 4000-6000 m to the south of Walvis Ridge (Fig.2). For these currents to continue north of the ridge for ~2000 km and to reach the study site, with water depths of 800-1500 m water depths, would likely have been captured in other proxy records from the region, which it has not.

On the other hand, the concept of a flow toward the south-southwest or west-southwest in forming the sediment wave is contextually more appropriate for this setting. Considering the geography and oceanography of the study area, such as: i) minimum Coriolis Effect due to location near to the equator, (ii) regional geomorphology – adjacent to the Congo Fan (~150 km) and continental shelf (~70 km), and (iii) location at slope margin and water depths 800-1700 m, there are several possible origins that could generate flows in these directions. This includes overflow of the Congo Canyon, cascading off shelf water, and internal waves or a combination of some or all (Fig.16). In normal circumstances, overflow of the Congo Canyon is limited by the deep entrenchment of the high canyon sidewalls (see the Congo Fan section). However, the region is subjected to arid/humid transition periods associated with the West African monsoon. During the transition period, the vegetation phase would lag behind the precipitation phase, as a consequence there would be a time when there is an onset between high river discharge into the Congo Canyon system from high precipitation levels and the minimum vegetation cover and up-fan avulsions (Picot et al., 2016, 2019). High-turbidity capacity that is coeval with up-fan avulsion thickens the turbidity flow volume (e.g., Hiscott et al., 1997), increasing possibility for overflow events to occur along the Congo Canyon/Channel in these periods. Meanwhile, cascading flow of the shelf water can travel across the slope into the study area due to climatic disruption such as salinisation, and/or large storms (cf., Anderskov et al., 2010; Canals et al., 2006; Hernández-Molina et al., 2016; Lonergan et al., 2013). Such cascading flow may also contribute to increase the turbidity flow capacity of the Congo Fan (cf., Canals et al., 2006; Puig et al., 2008). Lastly, interfaces between different water-masses occur in the water depths where the study site is located (Table.3). Any disruption of these water-mass interfaces could possibly generate internal waves that cause

shoaling and breaking on the continental slope, potentially generating downslope or upslope currents (Hernández-Molina et al., 2016; Pomar et al., 2012).

5.2.3. Implications for similar ridge-furrow structures in the region

Although not always specifically described, similar ridge-furrow structures can be observed in a number of previous 3D-seismic studies from Gabon to the Kwanza Basin (see digitised furrows on Fig.1) (Gay et al., 2004; Jatiault et al., 2019; Jones et al., 2014; Lonergan et al., 2013; Maia et al., 2016; Serié et al., 2017). Details of these observed furrows are provided in Table 2. The observed structures in these studies share broad similarities with those in this study – e.g. the dimensions, the obliquity of the ridge-furrow orientation to the local slope contours, the wavelength (or distance between furrows) ranging from tens to thousands of meters, and the location of the structures in water depths range of 800-2000 m. The similarities between the ridge-furrow structures identified across the West Africa slope margin means that they may share a similar origin as the sediment waves described above.

5.3. Palaeoceanography implication

Although it is important for elucidating the impact of key climatic events and its wider influence on ocean-atmospheric-and-climate interactions during the Quaternary (e.g., the 40- to-100 kyr shift in glacial cycle during the MPT), the reconstruction of the regional palaeoceanographic regime in the study region remains unresolved. When the ridge-furrow structures are interpreted as sediment waves, they can then be used to reconstruct the bottom currents regime over this time period back to their first emergence on the Gelasian surface.

As given above, the ridge-furrow structures as sediment waves could result from a flow toward the south-southwest or west-southwest, dependent upon the flow regime (Fig. 14c-d, i-j). If the origin is overflow from the Congo Canyon, it would then suggest that a thickening of turbidity flow over the Congo Canyon occurred during certain periods of the Quaternary. This thickening would have caused sufficient overflow to overcome the entrenchment by the high canyon sidewalls. The overflow would then travel through the study area, which is distal to the

canyon (~150 km away). If the origin is from cascading off shelf water, it would suggest that palaeoclimatic conditions allowed salinisation and/or possible cooling to occur. In such a scenario, dense over the surface waters, extreme conditions during large storms during low-sea level, or overspilling from alongshore shelf currents could trigger the cascading process (e.g., Canals et al., 2006; Hernández-Molina et al., 2016; Lonergan et al., 2013). If the origin is from internal waves, it would then require the presence of physical processes that could trigger the disruption of horizontal density surfaces within a stratified water column (see Hernández-Molina et al. (2016) for a list of examples of physical processes that could trigger internal wave to occur). It is not clear what could have caused this exact disruption in the study area, other than to hypothesise large storms or propagating deep oceanic waves. If the origin is a combination of them, those events above would then occur simultaneously, which may be triggered by the same palaeo-climatic events, for instance changing in West African monsoon. More work needs to be carried out to sample the sedimentary characteristics of the ridge-furrow structures to elucidate any associated palaeoclimatic information in order to determine which scenario is the most likely cause of these features.

6. CONCLUSION

Fields of ridge-furrow structures were identified in the shallow interval that extends from ~Top Gelasian (1.8 Ma) to present-day in age from 3D seismic cube analysis on the continental slope of the Lower Congo Basin. Here, geometrical descriptions were derived from the observation of furrows that are seismically more discernible than the subtle ridges. The geometrical description demonstrates that the ridge-furrow structures have a similar characteristic to those formed in deepwater sediment wave fields elsewhere. Based on the contextual analysis that consider the present and past oceanographic regime in the area, it is more likely that the identified ridge-furrow structures were formed by flows with a specific flow regime of $1 < Fr_{max} < 2$. The exact oceanographic origin of these features requires further work and likely relates to longshore currents cascading off the shelf, distal overflows from the Congo Canyon, breaking of internal waves or a mixture of these processes. This new recognition of

the Lower Congo Basin ridge-furrow structures as sediment waves provides an alternative interpretation of similar structures in the continental slope that have previously been interpreted as erosional scours, or, as in a case study to the north side of the Congo Canyon, an early phase of polygonal faults formation. The identification of the orientation and migration of the sediment waves related ridge-furrow structures in continental slope may then be used as a tool to describe the palaeoceanography in those areas (e.g., mean flow direction and range of magnitude) with the caveat that ridge-trough structures may stack in a downslope or upslope or aggradational pattern, with different implications for the dominant bottom current regime.

7. DATA AVAILABILITY

The seismic data used within this study were kindly provided by Petroleum Geo-Services (PGS) and *Agência Nacional de Petróleo, Gás e Biocombustíveis* (ANPG). To access these data, the companies and/or the Angola authorities will need to be contacted directly.

8. ACKNOWLEDGEMENTS

The authors would like to thank PGS and ANPG for the provision of the 3D seismic dataset and its allowance in publishing the research as well as ESRI, Schlumberger, and Eliis for the provision of ArcGIS, Petrel, and Paleoscan research-based license software respectively. The authors also thank Rufus Brunt, Jonathan Bull, Elda Miramontes, Ardiansyah Koeshidayatullah, and two anonymous reviewers for the constructive input to the manuscript. HP was funded by the Lembaga Pengelola Dana Pendidikan (LPDP) grant 20160222025510. AMWN was supported by NERC grant NE/R013675/1.

9. REFERENCES

595 Anderskov, K., Surlyk, F., Huuse, M., Lykke-Andersen, H., Bjerager, M., Tang, C., 2010. Sediment waves with a
 596 biogenic twist in Pleistocene cool water carbonates, Great Australian Bight. *Marine Geology* 278, 122-
 597 139.

598 Anderson, J., Cartwright, J., Drysdall, S., Vivian, N., 2000. Controls on turbidite sand deposition during gravity-driven
 599 extension of a passive margin: examples from Miocene sediments in Block 4, Angola. *Marine and*
 600 *Petroleum Geology* 17, 1165-1203.

601 Andresen, K.J., Huuse, M., 2011. 'Bulls-eye' pockmarks and polygonal faulting in the Lower Congo Basin: relative
 602 timing and implications for fluid expulsion during shallow burial. *Marine Geology* 279, 111-127.

603 Anka, Z., Seranne, M., Lopez, M., Scheck-Wenderoth, M., Savoye, B., 2009. The long-term evolution of the Congo
 604 deep-sea fan: A basin-wide view of the interaction between a giant submarine fan and a mature
 605 passive margin (ZaiAngo project). *Tectonophysics* 470, 42-56.

606 Arhan, M., Mercier, H., Park, Y.-H., 2003. On the deep water circulation of the eastern South Atlantic Ocean. *Deep*
 607 *Sea Research Part I: Oceanographic Research Papers* 50, 889-916.

608 Babonneau, N., Savoye, B., Cremer, M., Bez, M., 2004. Multiple terraces within the deep incised Zaire Valley (ZaiAngo
 609 Project): are they confined levees? *Geological Society, London, Special Publications* 222, 91-114.

610 Babonneau, N., Savoye, B., Cremer, M., Klein, B., 2002. Morphology and architecture of the present canyon and
 611 channel system of the Zaire deep-sea fan. *Marine and Petroleum Geology* 19, 445-467.

612 Bacon, M., Simm, R., Redshaw, T., 2007. 3-D seismic interpretation. Cambridge University Press.

613 Bartek, L.R., Vail, P., Anderson, J., Emmet, P., Wu, S., 1991. Effect of Cenozoic ice sheet fluctuations in Antarctica on
 614 the stratigraphic signature of the Neogene. *Journal of Geophysical Research: Solid Earth* 96, 6753-
 615 6778.

616 Bell, D.B., Jung, S.J., Kroon, D., 2015. The Plio-Pleistocene development of Atlantic deep-water circulation and its
 617 influence on climate trends. *Quaternary Science Reviews* 123, 265-282.

618 Berger, W., Wefer, G., Richter, C., Lange, C., Giraudeau, J., Hermelin, O., Party, S.S., 1998. The Angola-Benguela
 619 Upwelling System: Paleoceanographic Synthesis of Shipboard Results From LEG 175, in: Wefer, G.,
 620 Berger, W.H., Richter, C., al., e. (Eds.), *Proceedings Ocean Drilling Program, Initial Reports*, pp. 505-
 621 531.

622 Biscara, L., Mulder, T., Gonthier, E., Cremer, M., Faugères, J.-C., Garlan, T., 2010. Migrating submarine furrows on
623 Gabonese margin (West Africa) from Miocene to present: influence of bottom currents. *Geo-temas*
624 11, 21-22.

625 Bolli, H., Ryan, W., Foresman, J., Hottman, W., Kagami, H., Longoria, J., McKnight, B., Melguen, M., Natland, J., Proto-
626 Decima, F., 1978. Angola continental margin—Sites 364 and 365. Initial Reports of the Deep Sea
627 Drilling Project 40, 357-390.

628 Bonaldo, D., Benetazzo, A., Bergamasco, A., Campiani, E., Foglini, F., Sclavo, M., Trincardi, F., Carniel, S., 2016.
629 Interactions among Adriatic continental margin morphology, deep circulation and bedform patterns.
630 *Marine Geology* 375, 82-98.

631 Brice, S.E., Cochran, M.D., Pardo, G., Edwards, A.D., 1982. Tectonics and Sedimentation of the South Atlantic Rift
632 Sequence: Cabinda, Angola: Rifted Margins: Field Investigations of Margin Structure and
633 Stratigraphy, *M 34: Studies in Continental Margin Geology*. AAPG, pp. 5-18.

634 Broucke, O., Temple, F., Rouby, D., Robin, C., Calassou, S., Nalpas, T., Guillocheau, F., 2004. The role of deformation
635 processes on the geometry of mud-dominated turbiditic systems, Oligocene and Lower–Middle
636 Miocene of the Lower Congo basin (West African Margin). *Marine and Petroleum Geology* 21, 327-
637 348.

638 Buckley, F., 2017. A glaciogenic sequence from the Early Pleistocene of the Central North Sea. *Journal of Quaternary*
639 *Science* 32, 145-168.

640 Canals, M., Puig, P., de Madron, X.D., Heussner, S., Palanques, A., Fabres, J., 2006. Flushing submarine canyons.
641 *Nature* 444, 354-357.

642 Cartigny, M.J., Postma, G., 2017. Turbidity current bedforms, *Atlas of bedforms in the Western Mediterranean*.
643 Springer, pp. 29-33.

644 Cartigny, M.J., Postma, G., van den Berg, J.H., Mastbergen, D.R., 2011. A comparative study of sediment waves and
645 cyclic steps based on geometries, internal structures and numerical modeling. *Marine Geology* 280,
646 40-56.

647 Cartwright, J., 1995. Seismic-Stratigraphical Analysis of Large-Scale Ridge–Trough Sedimentary Structures in the
648 Late Miocene to Early Pliocene of the Central North Sea. *Sedimentary Facies Analysis: A Tribute to*
649 *the Research and Teaching of Harold G. Reading*, 283-303.

650 Cartwright, J., 2011. Diagenetically induced shear failure of fine-grained sediments and the development of
 651 polygonal fault systems. *Marine and Petroleum Geology* 28, 1593-1610.

652 Dorokhov, D., Dorokhova, E., Sivkov, V., 2018. Iceberg and ice-keel ploughmarks on the Gdansk-Gotland Sill (south-
 653 eastern Baltic Sea). *Geo-Marine Letters* 38, 83-94.

654 Droz, L., Marsset, T., Ondreas, H., Lopez, M., Savoye, B., Spy-Anderson, F.-L., 2003. Architecture of an active mud-
 655 rich turbidite system: The Zaire Fan (Congo–Angola margin southeast Atlantic) Results from ZaiAngo
 656 1 and 2 cruises. *AAPG bulletin* 87, 1145-1168.

657 Ercilla, G., Juan, C., Hernandez-Molina, F.J., Bruno, M., Estrada, F., Alonso, B., Casas, D., lí Farran, M., Llave, E., Garcia,
 658 M., 2016. Significance of bottom currents in deep-sea morphodynamics: an example from the
 659 Alboran Sea. *Marine Geology* 378, 157-170.

660 Faugères, J.-C., Stow, D.A., Imbert, P., Viana, A., 1999. Seismic features diagnostic of contourite drifts. *Marine*
 661 *Geology* 162, 1-38.

662 Flood, R.D., 1983. Classification of sedimentary furrows and a model for furrow initiation and evolution. *Geological*
 663 *Society of America Bulletin* 94, 630-639.

664 Flood, R.D., 1994. Abyssal bedforms as indicators of changing bottom current flow: examples from the US East
 665 Coast continental rise. *Paleoceanography* 9, 1049-1060.

666 Fort, X., Brun, J.-P., Chauvel, F., 2004. Salt tectonics on the Angolan margin, synsedimentary deformation processes.
 667 *AAPG bulletin* 88, 1523-1544.

668 García, M., Hernández-Molina, F.J., Llave, E., Stow, D., León, R., Fernández-Puga, M., Del Río, V.D., Somoza, L., 2009.
 669 Contourite erosive features caused by the Mediterranean Outflow Water in the Gulf of Cadiz:
 670 Quaternary tectonic and oceanographic implications. *Marine Geology* 257, 24-40.

671 García, M., Lobo, F.J., Maldonado, A., Hernández-Molina, F.J., Bohoyo, F., Pérez, L.F., 2016. High-resolution seismic
 672 stratigraphy and morphology of the Scan Basin contourite fan, southern Scotia Sea, Antarctica.
 673 *Marine Geology* 378, 361-373.

674 Garzoli, S.L., Dong, S., Fine, R., Meinen, C.S., Perez, R.C., Schmid, C., Van Sebille, E., Yao, Q., 2015. The fate of the
 675 deep western boundary current in the South Atlantic. *Deep Sea Research Part I: Oceanographic*
 676 *Research Papers* 103, 125-136.

677 Gay, A., Lopez, M., Berndt, C., Seranne, M., 2007. Geological controls on focused fluid flow associated with seafloor
 678 seeps in the Lower Congo Basin. *Marine Geology* 244, 68-92.

679 Gay, A., Lopez, M., Cochonat, P., Sermondadaz, G., 2004. Polygonal faults-furrows system related to early stages of
680 compaction–upper Miocene to recent sediments of the Lower Congo Basin. *Basin Research* 16, 101-
681 116.

682 Gee, M., Gawthorpe, R., Friedmann, S., 2006. Triggering and evolution of a giant submarine landslide, offshore
683 Angola, revealed by 3D seismic stratigraphy and geomorphology. *Journal of Sedimentary Research*
684 76, 9-19.

685 Gruetzner, J., Uenzelmann-Neben, G., Franke, D., Arndt, J.E., 2014. Slowdown of Circumpolar Deepwater flow during
686 the Late Neogene: evidence from a mudwave field at the Argentine continental slope. *Geophysical*
687 *Research Letters* 41, 2070-2076.

688 Guiavarc'h, C., Treguier, A.M., Vangriesheim, A., 2008. Remotely forced biweekly deep oscillations on the continental
689 slope of the Gulf of Guinea. *Journal of Geophysical Research: Oceans* 113.

690 Guiavarc'h, C., Tréguier, A.-M., Vangriesheim, A., 2009. Deep currents in the Gulf of Guinea: along slope propagation
691 of intraseasonal waves. *Ocean Science* 5, 141-153.

692 Halberstadt, A.R.W., Simkins, L.M., Greenwood, S.L., Anderson, J.B., 2016. Past ice-sheet behaviour: retreat scenarios
693 and changing controls in the Ross Sea, Antarctica. *The Cryosphere* 10, 1003-1020.

694 Hardman-Mountford, N., Richardson, A., Agenbag, J., Hagen, E., Nykjaer, L., Shillington, F., Villacastin, C., 2003.
695 Ocean climate of the South East Atlantic observed from satellite data and wind models. *Progress in*
696 *Oceanography* 59, 181-221.

697 Hernández-Molina, F.J., Llave, E., Stow, D., García, M., Somoza, L., Vázquez, J.T., Lobo, F., Maestro, A., Del Río, V.D.,
698 León, R., 2006. The contourite depositional system of the Gulf of Cadiz: a sedimentary model related
699 to the bottom current activity of the Mediterranean outflow water and its interaction with the
700 continental margin. *Deep Sea Research Part II: Topical Studies in Oceanography* 53, 1420-1463.

701 Hernández-Molina, F.J., Llave, E., Stow, D.A.V., 2008. Chapter 19 Continental Slope Contourites, in: Rebesco, M.,
702 Camerlenghi, A. (Eds.), *Developments in Sedimentology*. Elsevier, pp. 379-408.

703 Hernández-Molina, F.J., Soto, M., Piola, A.R., Tomasini, J., Preu, B., Thompson, P., Badalini, G., Creaser, A., Violante,
704 R.A., Morales, E., 2016. A contourite depositional system along the Uruguayan continental margin:
705 sedimentary, oceanographic and paleoceanographic implications. *Marine Geology* 378, 333-349.

706 Hill, J.C., Gayes, P.T., Driscoll, N.W., Johnstone, E.A., Sedberry, G.R., 2008. Iceberg scours along the southern US
707 Atlantic margin. *Geology* 36, 447-450.

708 Hiscott, R.N., Hall, F.R., Pirmez, C., 1997. Turbidity-current overspill from the Amazon Channel: texture of the
 709 silt/sand load, paleoflow from anisotropy of magnetic susceptibility, and implications for flow
 710 processes, *Proceedings-Ocean Drilling Program Scientific Results*. NATIONAL SCIENCE
 711 FOUNDATION, pp. 53-78.

712 Hohbein, M., Cartwright, J., 2006. 3D seismic analysis of the West Shetland Drift system: Implications for Late
 713 Neogene palaeoceanography of the NE Atlantic. *Marine Geology* 230, 1-20.

714 Holfort, J., Siedler, G., 2001. The meridional oceanic transports of heat and nutrients in the South Atlantic. *Journal*
 715 *of Physical Oceanography* 31, 5-29.

716 Hopkins, J., Lucas, M., Dufau, C., Sutton, M., Stum, J., Lauret, O., Channelliere, C., 2013. Detection and variability of
 717 the Congo River plume from satellite derived sea surface temperature, salinity, ocean colour and sea
 718 level. *Remote Sensing of Environment* 139, 365-385.

719 Jatiault, R., Dhont, D., Loncke, L., de Madron, X.D., Dubucq, D., Channelliere, C., Bourrin, F., 2018. Deflection of natural
 720 oil droplets through the water column in deep-water environments: The case of the Lower Congo
 721 Basin. *Deep Sea Research Part I: Oceanographic Research Papers* 136, 44-61.

722 Jatiault, R., Dhont, D., Loncke, L., Dubucq, D., 2017. Monitoring of natural oil seepage in the Lower Congo Basin
 723 using SAR observations. *Remote Sensing of Environment* 191, 258-272.

724 Jatiault, R., Loncke, L., Dhont, D., Dubucq, D., Imbert, P., 2019. Geophysical characterisation of active thermogenic
 725 oil seeps in the salt province of the lower Congo basin. Part II: A regional validation. *Marine and*
 726 *Petroleum Geology* 103, 773-791.

727 Jones, D.O., Walls, A., Clare, M., Fiske, M.S., Weiland, R.J., O'Brien, R., Touzel, D.F., 2014. Asphalt mounds and
 728 associated biota on the Angolan margin. *Deep Sea Research Part I: Oceanographic Research Papers*
 729 94, 124-136.

730 Karner, G.D., Driscoll, N.W., McGinnis, J.P., Brumbaugh, W.D., Cameron, N.R., 1997. Tectonic significance of syn-rift
 731 sediment packages across the Gabon-Cabinda continental margin. *Marine and Petroleum Geology*
 732 14, 973-1000.

733 Kilhams, B., McArthur, A., Huuse, M., Ita, E., Hartley, A., 2011. Enigmatic large-scale furrows of Miocene to Pliocene
 734 age from the central North Sea: current-scoured pockmarks? *Geo-Marine Letters* 31, 437-449.

735 Knutz, P.C., Sicre, M.A., Ebbesen, H., Christiansen, S., Kuijpers, A., 2011. Multiple-stage deglacial retreat of the
736 southern Greenland Ice Sheet linked with Irminger Current warm water transport. *Paleoceanography*
737 26.

738 Lamb, R.M., Huuse, M., Stewart, M., 2017. Early Quaternary sedimentary processes and palaeoenvironments in the
739 central North Sea. *Journal of Quaternary Science* 32, 127-144.

740 Laurent, D., Marsset, T., Droz, L., Granjeon, D., Molliex, S., Picot, M., Rabineau, M., 2020. 4D forward stratigraphic
741 modelling of the Late Quaternary Congo deep-sea fan: Role of climate/vegetation coupling in
742 architectural evolution. *Marine Geology* 429, 106334.

743 Lobo, F.J., Hernández-Molina, F.J., Bohoyo, F., Galindo-Zaldívar, J., Maldonado, A., Martos, Y., Rodríguez-Fernández,
744 J., Somoza, L., Vázquez, J.T., 2011. Furrows in the southern Scan Basin, Antarctica: interplay between
745 tectonic and oceanographic influences. *Geo-Marine Letters* 31, 451-464.

746 Lonergan, L., Jamin, N.H., Jackson, C.A.L., Johnson, H.D., 2013. U-shaped slope gully systems and sediment waves
747 on the passive margin of Gabon (West Africa). *Marine Geology* 337, 80-97.

748 Maia, A.R., Cartwright, J., Andersen, E., 2016. Shallow plumbing systems inferred from spatial analysis of pockmark
749 arrays. *Marine and Petroleum Geology* 77, 865-881.

750 Manley, P.L., Flood, R.D., 1993. Paleoflow history determined from mudwave migration: Argentine Basin. *Deep Sea*
751 *Research Part II: Topical Studies in Oceanography* 40, 1033-1055.

752 Marsset, T., Droz, L., Dennielou, B., Pichon, E., 2009. Cycles in the architecture of the Quaternary Zaire turbidite
753 system: a possible link with climate. *External Controls on Deep-Water Depositional Systems. SEPM*
754 *Special Publication* 92, 89-106.

755 Marton, L.G., Tari, G.C., Lehmann, C.T., 2000. Evolution of the Angolan Passive Margin, West Africa, With Emphasis
756 on Post-Salt Structural Styles. *Atlantic rifts and continental margins*, 129-149.

757 Masson, D., Wynn, R., Bett, B., 2004. Sedimentary environment of the Faroe-Shetland and Faroe Bank Channels,
758 north-east Atlantic, and the use of bedforms as indicators of bottom current velocity in the deep
759 ocean. *Sedimentology* 51, 1207-1241.

760 McCave, I., 1971. Wave effectiveness at the sea bed and its relationship to bed-forms and deposition of mud. *Journal*
761 *of Sedimentary Research* 41, 89-96.

762 McCave, I., 2017. Formation of sediment waves by turbidity currents and geostrophic flows: A discussion. *Marine*
763 *Geology* 390, 89-93.

764 Metz, J., Dowdeswell, J., Woodworth-Lynas, C., 2008. Sea-floor scour at the mouth of Hudson Strait by deep-keeled
765 icebergs from the Laurentide Ice Sheet. *Marine Geology* 253, 149-159.

766 Miramontes, E., Jouet, G., Thereau, E., Bruno, M., Penven, P., Guerin, C., Le Roy, P., Droz, L., Jorry, S.J., Hernández-
767 Molina, F.J., 2020. The impact of internal waves on upper continental slopes: insights from the
768 Mozambican margin (southwest Indian Ocean). *Earth Surface Processes and Landforms* 45, 1469-
769 1482.

770 Miramontes, E., Thiéblemont, A., Babonneau, N., Penven, P., Raissou, F., Droz, L., Jorry, S.J., Fierens, R., Counts, J.W.,
771 Wilckens, H., 2021. Contourite and mixed turbidite-contourite systems in the Mozambique Channel
772 (SW Indian Ocean): Link between geometry, sediment characteristics and modelled bottom currents.
773 *Marine Geology*, 106502.

774 Newton, A., Huuse, M., Brocklehurst, S., 2018. A persistent Norwegian Atlantic current through the Pleistocene
775 glacials. *Geophysical Research Letters* 45, 5599-5608.

776 Newton, A.M., Huuse, M., Brocklehurst, S.H., 2016. Buried iceberg scours reveal reduced North Atlantic Current
777 during the stage 12 deglacial. *Nature communications* 7, 10927.

778 Nugraha, H.D., Jackson, C.A., Johnson, H.D., Hodgson, D.M., Reeve, M.T., 2019. Tectonic and oceanographic process
779 interactions archived in Late Cretaceous to Present deep-marine stratigraphy on the Exmouth
780 Plateau, offshore NW Australia. *Basin Research* 31, 405-430.

781 Oluboyo, A., Gawthorpe, R., Bakke, K., Hadler-Jacobsen, F., 2014. Salt tectonic controls on deep-water turbidite
782 depositional systems: Miocene, southwestern Lower Congo Basin, offshore Angola. *Basin Research*
783 26, 597-620.

784 Palanques, A., de Madron, X.D., Puig, P., Fabres, J., Guillén, J., Calafat, A., Canals, M., Heussner, S., Bonnin, J., 2006.
785 Suspended sediment fluxes and transport processes in the Gulf of Lions submarine canyons. The role
786 of storms and dense water cascading. *Marine Geology* 234, 43-61.

787 Pena, L.D., Goldstein, S.L., 2014. Thermohaline circulation crisis and impacts during the mid-Pleistocene transition.
788 *Science* 345, 318-322.

789 Picot, M., Droz, L., Marsset, T., Dennielou, B., Bez, M., 2016. Controls on turbidite sedimentation: insights from a
790 quantitative approach of submarine channel and lobe architecture (Late Quaternary Congo Fan).
791 *Marine and Petroleum Geology* 72, 423-446.

792 Picot, M., Marsset, T., Droz, L., Dennielou, B., Baudin, F., Hermoso, M., De Rafélis, M., Sionneau, T., Cremer, M.,
 793 Laurent, D., 2019. Monsoon control on channel avulsions in the Late Quaternary Congo Fan.
 794 Quaternary Science Reviews 204, 149-171.

795 Pomar, L., Morsilli, M., Hallock, P., Bádenas, B., 2012. Internal waves, an under-explored source of turbulence events
 796 in the sedimentary record. Earth-Science Reviews 111, 56-81.

797 Posamentier, H.W., 2004. Seismic Geomorphology: Imaging Elements of Depositional Systems from Shelf to Deep
 798 Basin Using 3D Seismic Data: Implications for Exploration and Development. Geological Society,
 799 London, Memoirs 29, 11-24.

800 Posamentier, H.W., Kolla, V., 2003. Seismic geomorphology and stratigraphy of depositional elements in deep-water
 801 settings. Journal of Sedimentary Research 73, 367-388.

802 Pufahl, P., Maslin, M., Anderson, L., Brüchert, V., Jansen, F., Lin, H., Perez, M., Vidal, L., Party10, S.S., 1998. 18.
 803 LITHOSTRATIGRAPHIC SUMMARY FOR LEG 175: ANGOLA-BENGUELA UPWELLING SYSTEM1,
 804 Proceedings Ocean Drilling Program, Initial Reports, pp. 533-542.

805 Puig, P., Palanques, A., Orange, D., Lastras, G., Canals, M., 2008. Dense shelf water cascades and sedimentary furrow
 806 formation in the Cap de Creus Canyon, northwestern Mediterranean Sea. Continental Shelf Research
 807 28, 2017-2030.

808 Rebesco, M., Hernández-Molina, F.J., Van Rooij, D., Wåhlin, A., 2014. Contourites and associated sediments
 809 controlled by deep-water circulation processes: state-of-the-art and future considerations. Marine
 810 Geology 352, 111-154.

811 Savoye, B., Babonneau, N., Dennielou, B., Bez, M., 2009. Geological overview of the Angola–Congo margin, the
 812 Congo deep-sea fan and its submarine valleys. Deep Sea Research Part II: Topical Studies in
 813 Oceanography 56, 2169-2182.

814 Schollnberger, E.M., 2001. Seismic sequence stratigraphy of the Lower Congo, Kwanza, and Benguela basins,
 815 offshore Angola, Africa. Rice University.

816 Séranne, M., 1999. Early Oligocene stratigraphic turnover on the west Africa continental margin: a signature of the
 817 Tertiary greenhouse-to-icehouse transition? Terra Nova-Oxford 11, 135-140.

818 Séranne, M., Nzé Abeigne, C.-R., 1999. Oligocene to Holocene sediment drifts and bottom currents on the slope of
 819 Gabon continental margin (west Africa): Consequences for sedimentation and southeast Atlantic
 820 upwelling. Sedimentary Geology 128, 179-199.

821 Séranne, M., Seguret, M., Fauchier, M., 1992. Seismic super-units and post-rift evolution of the continental passive
 822 margin of southern Gabon. *Bulletin de la Société géologique de France* 163, 135-146.

823 Serié, C., Huuse, M., Schødt, N.H., Brooks, J.M., Williams, A., 2017. Subsurface fluid flow in the deep-water Kwanza
 824 Basin, offshore Angola. *Basin Research* 29, 149-179.

825 Shin, H., Santamarina, J.C., Cartwright, J.A., 2008. Contraction-driven shear failure in compacting uncemented
 826 sediments. *Geology* 36, 931-934.

827 Stow, D.A., Hernández-Molina, F.J., Llave, E., Sayago-Gil, M., Díaz del Río, V., Branson, A., 2009. Bedform-velocity
 828 matrix: the estimation of bottom current velocity from bedform observations. *Geology* 37, 327-330.

829 Stramma, L., England, M., 1999. On the water masses and mean circulation of the South Atlantic Ocean. *Journal of*
 830 *Geophysical Research: Oceans* 104, 20863-20883.

831 Stramma, L., Fischer, J., Brandt, P., Schott, F., 2003. Circulation, variability and near-equatorial meridional flow in the
 832 central tropical Atlantic, Elsevier Oceanography Series. Elsevier, pp. 1-22.

833 Stramma, L., Schott, F., 1999. The mean flow field of the tropical Atlantic Ocean. *Deep Sea Research Part II: Topical*
 834 *Studies in Oceanography* 46, 279-303.

835 Sun, Q., Cartwright, J., Wu, S., Zhong, G., Wang, S., Zhang, H., 2016. Submarine erosional troughs in the northern
 836 South China Sea: Evidence for Early Miocene deepwater circulation and paleoceanographic change.
 837 *Marine and Petroleum Geology* 77, 75-91.

838 Svendsen, L., Kvamstø, N.G., Keenlyside, N., 2014. Weakening AMOC connects Equatorial Atlantic and Pacific
 839 interannual variability. *Climate dynamics* 43, 2931-2941.

840 Tari, G., Molnar, J., Ashton, P., 2003. Examples of salt tectonics from West Africa: a comparative approach. *Geological*
 841 *Society, London, Special Publications* 207, 85-104.

842 Tokinaga, H., Xie, S.-P., 2011. Weakening of the equatorial Atlantic cold tongue over the past six decades. *Nature*
 843 *Geoscience* 4, 222.

844 Uchupi, E., 1992. Angola Basin: geohistory and construction of the continental rise. *Geologic Evolution of Atlantic*
 845 *Continental Rifts*. Nostrand Reinhold, New York, 77-99.

846 Uenzelmann-Neben, G., 1998. Neogene sedimentation history of the Congo Fan. *Marine and Petroleum Geology*
 847 15, 635-650.

848 Uenzelmann-Neben, G., Spiess, V., Bleil, U., 1997. A seismic reconnaissance survey of the northern Congo Fan.
 849 *Marine Geology* 140, 283-306.

850 Valle, P.J., Gjelberg, J.G., Helland-Hansen, W., 2001. Tectonostratigraphic development in the eastern Lower Congo
851 Basin, offshore Angola, west Africa. *Marine and Petroleum Geology* 18, 909-927.

852 Vangriesheim, A., Treguier, A.M., Andre, G., 2005. Biweekly current oscillations on the continental slope of the Gulf
853 of Guinea. *Deep Sea Research Part I: Oceanographic Research Papers* 52, 2168-2183.

854 Venz, K.A., Hodell, D.A., 2002. New evidence for changes in Plio–Pleistocene deep water circulation from Southern
855 Ocean ODP Leg 177 Site 1090. *Palaeogeography, Palaeoclimatology, Palaeoecology* 182, 197-220.

856 Wynn, R.B., Stow, D.A.V., 2002. Classification and characterisation of deep-water sediment waves. *Marine Geology*
857 192, 7-22.

858 Xie, S.-P., Carton, J.A., 2004. Tropical Atlantic variability: Patterns, mechanisms, and impacts. *Earth's Climate: The*
859 *Ocean-Atmosphere Interaction, Geophys. Monogr* 147, 121-142.

860

861

TABLE FOR MANUSCRIPT

TITLE:

*MIDDLE TO LATE PLEISTOCENE PALEOCEANOGRAPHY INFERRED
FROM RIDGE-FURROW STRUCTURES ON THE CONTINENTAL SLOPE OF
THE LOWER CONGO BASIN*

Hugo Putuhena^{1*}

Andrew M.W. Newton²

Joe Cartwright³

Mads Huuse¹

Manuscript submitted to:

Marine Geology – special issue

* hugo.putuhena@manchester.ac.uk

*1) Department of Earth and Environmental Sciences, The University of Manchester, M13 9PL,
Manchester, United Kingdom*

*2) School of Natural and Built Environment, Queen's University Belfast, BT7 1NN, Belfast,
United Kingdom*

3) Department of Earth Sciences, University of Oxford, OX1 3AN, Oxford, United Kingdom

882 Table.1. List of furrow structures observations worldwide and what was defined as the origin for each of them. * is given for the references that
883 were conducted using a 3D seismic observation.

884

| Definition of Furrows | Occurrence | Dimension | | | Linear/ Arcuate/ Sinuous | Orientation | Migration through time | Spatial characteristic | Flow velocity that may generate the furrows in muddy environments | References |
|--------------------------------------------------|--------------------------------------------------------------------------------------------------------------------------------------------------------------------------------------------------------------------------------------------------------------------------------------------------------------------------------------------------------------------------------------------------------------------------------------------|------------|------------------|--------------------------|--------------------------------|----------------------------------------------------------------------------------------------------------------------------------------------|-------------------------------------------------------------------------------------------------------------------------------------------------------------------------------------------------------------------------------|----------------------------------------------------------------------------------------------------------------------------------------------------------------------------------------------------------------|----------------------------------------------------------------------------|------------------------------------------------------------------------------------------------------------------------------------------------------------------------------------------------------------------------------------------------------------------------------------------------------------------------------------------------------------------------------------------------------------------------------------------------------------------|
| | | Length | Wide | Depth | | | | | | |
| As the bottom- currents erosional features | Various locations: (i) buried in the early Quaternary of the central North Sea basin; in the Late Cretaceous in Exmouth Plateau, offshore NW Australia; in the early-Miocene in the northern South China Sea; (ii) on the seabed in the Faroe-Shetland and Faroe Bank Channels at water depths 800-1200 m; in the Adriatic basin at water depths 300-800 m; in the Gulf of Cadiz; in the Scan Basin, Antarctica at water depth 2700-3200 m | tens of km | tens of m - 3 km | a few tens of cm - 250 m | Linear/arcuate | Mostly parallel to the slope | Lateral (Coriolis related) migration--to the right of the flow direction in NH - <i>Lamb et al., 2017</i> ; and lateral (non-Coriolis related) migration--to the left of the flow direction in NH - <i>Sun et al., 2016</i> ; | In the group with tens to hundreds of units/regularly spaced; Some with relatively large dimension were found isolated and associated with high bathymetry structures such as mud volcanoes/diapir/ridges/etc. | >0.3 m/s (<i>Stow et al., 2009</i>) | <i>Rebesco et al., 2014</i> ; <i>Hernández-Molina et al., 2008</i> ; <i>Cartwright, 1995</i> ; <i>Lamb et al., 2017*</i> ; <i>Buckley, 2017*</i> ; <i>Masson et al., 2004</i> ; <i>Knutz et al., 2011*</i> ; <i>Bonaldo et al., 2016</i> ; <i>Nugraha et al., 2019*</i> ; <i>Lobo et al., 2011</i> ; <i>García et al., 2009, 2016</i> ; <i>Perez et al., 2014, Sun et al., 2016*</i> ; <i>Hernández-Molina et al., 2006</i> ; <i>Ercilla et al., 2016</i> ; etc. |
| As the iceberg/stamukhi erosional features | Various locations in high-latitude areas on the present-day shelf to slope seabed surface, e.g., Norwegian Sea; Central basin-Ross sea at water depth 400-600 m; Offshore South Carolina at water depth 170-220 m; Gdansk-Gotland Sill at water depth 77-87 m; Hudson strait-Hatton basin at water depth 560-630 m | >10 km | 1-400 m | 1-20 m | Linear/arcuate | Dependent upon the position (e.g., they can be random, while on the others such as away from the ice sheet, they can be found quite uniform) | - | - | - | <i>Newton et al., 2016*</i> , <i>2018*</i> ; <i>Halberstadt et al., 2016</i> ; <i>Hill et al., 2008</i> ; <i>Dorokhov et al., 2018</i> ; <i>Metz et al., 2008</i> |

885

886

887 Table.1. (continued)

| Definition of Furrows | Occurrence | Dimension | | | Linear/ Arcuate/ Sinuous | Orientation | Migration through time | Spatial characteristic | Flow velocity that may generate the furrows in muddy environments | References |
|----------------------------------------------------------------|-------------------------------------------------------------------------------------------------------------------------------------------------------------------------------------------------------------------------------------------------------------------------------------------------------------------------------|-------------------|--------------------------------------------------------------------|--------------------------------------------------------------------------|--------------------------------|-----------------------------------------------------------|----------------------------------------------------------------------------------------------------------------------------------------------------|------------------------------------------------------------------------|-----------------------------------------------------------------------------|------------------------------------------------------------------------------------------------------|
| | | Length | Wide | Depth | | | | | | |
| As the turbidity- current erosional features | Various locations: (i) buried in the continental slope, e.g., buried on the Miocene age in the continental slope offshore the Lower Congo Basin and on the Pleistocene age offshore Borneo, Indonesia - ; (ii) on the seabed surface within the Cap de Creus Canyon | >10 km | up to 700 m | range from <20 - 40 m | Linear | Perpendicular ar to slope | - | In the group with up to tens of units/located in steep slope | - | <i>Gee et al., 2006*</i> ; <i>Posamentier and Kolla, 2003*</i> ; <i>Puig et al., 2008</i> |
| As the elongation of pockmarks | Buried on Miocene-to-Pliocene age in the North Sea Central Graben | up to 25 km | ~500 m - 3 km | 5-250 m | Linear | Parallel to slope | - | Located in the area where salt-diapir occurs | - | <i>Killhams et al. 2011*</i> |
| As the reworking of the abandoned u- shaped channel-like | From buried on the ~Oligocene age-to- Present-day seabed surface on the continental slope Offshore Gabon; water depths 500-1500 m; slope angle 0.2- 4.5 degree | 20-25 km | 2-8 km | 200 m | Linear | Perpendicular ar to slope | Direct Coriolis related migration-- lateral migration (to the left (right) in SH (NH)) towards the flow direction | Located in the steep slope above abandoned u-shaped channel-like | - | <i>Séranne and Nze Abeigne, 1999</i> ; <i>Biscara et al., 2010</i> |
| As the polygonal faults features | On the palaeo to present-day seabed surfaces in the interval starting from ~the Mid Pleistocene age surface on the continental slope offshore the Lower Congo Basin; water depths 1000-2000 m; slope angle <1 degree | up to a few km | 100-150 m? (based on the paper's figures observation) | a few meters? (based on the paper's figures observation) | Linear/slightly sinuous | Oblique but not perpendicular ar to the slope | - | In the group with up to hundreds of units/regularly spaced | - | <i>Gay et al., 2004*</i> |
| As the troughs of sediment waves | On the palaeo to present-day seabed surfaces in the interval started from ~the Mid Pleistocene age surface on the continental slope offshore the Lower Congo Basin; water depths 1000-1700 m; slope angle <1 degree; presence of similar furrows were also identified in offshore Gabon and Kwanza Basin | <0.5 - 5.5 km | 50-250 m | up to 10 m | Linear/slightly sinuous | Oblique but not perpendicular ar to the slope | Direct Coriolis related migration-- lateral migration (to the left (right) in SH (NH)) towards the flow direction | In the group with up to hundreds of units/regularly spaced | 5-20 cm/s <i>Manley & Flood, 1993</i> ; <i>Stow et al., 2009</i> | This study* |

889 Table.2. Dimension, orientation, spacing, and interval water depths occurrence of similar furrows identified in other seabed/3D seismic studies
890 from Gabon to Kwanza Basin. (*) are those studies where the furrows were not intentionally described in the papers, thus the dimensions given
891 there are based on the visual assessment from the paper figures.

| Paper publication | Basin | Furrows dimension | | | Furrows orientation | Furrows migration | Spacing | Interval Water Depth occurrence |
|------------------------|--------------------------------------------------------|-----------------------|---------------------|-----------------|---------------------|----------------------------|-----------------------------------|---------------------------------|
| | | Relief | Length | Width | | | | |
| Lonergan et al., 2013* | Gabon Basin | A few meters? | Hundreds of metres? | Tens of metres? | NW-SE | - | 200-500 m | 1100-1600 m |
| Gay et al., 2004, 2007 | Lower Congo Basin (to the north of the Congo Fan) | A few metres | 100-1100 m | Tens of metres | N-S | Aggrading only/almost zero | 1-3 km | 1000-2000 m |
| This study | Lower Congo Basin | 8-10 m | 500-5000 m | 60-80 m | WNW-ESE | To South-southwest | 50-1000 m | 800-1700 m |
| Jatiaux et al., 2019* | Lower Congo Basin (to the southwest of the study site) | | | | | | | 1400-1700 m |
| Jones et al., 2014* | Lower Congo Basin (to the west of the study site) | | | | | | | |
| Sérié et al., 2017* | Kwanza Basin | A few hundred meters? | Hundreds of metres? | Tens of metres? | Varying | - | Hundreds to a thousand of meters? | 1000-1400 m |

892

893

894 Table.3. Physical components and interval depths of circulating water masses in the water column of the study area. This information was
895 gathered from Arhan et al., 2003; Garzoli et al., 2015; Jatiault et al., 2018.

| Water mass | Driven currents | Velocity | Temperature | Salinity | Interval water depths |
|------------------------------------|-----------------------------------------------------------------------------------|---------------------------------|-------------|----------------|---------------------------------|
| River Discharge(RD) | Congo Plume (CP) | 20-50 cm/s (dispersing) | 24-26° C | 33.6-34.5 psu | 0-20 m |
| Surface Water (SW) | <ul style="list-style-type: none"> Angola Currents (AC) | 20-50 cm/s (southward) | 16-24° C | 36.4 psu | 0-300 m |
| | <ul style="list-style-type: none"> Benguela Coastal Currents (BCC) | 20-50 cm/s (northward) | colder | Lower salinity | Surface-subsurface (Beneath AC) |
| Atlantic Intermediate Water (AAIW) | South Intermediate Counter Currents (SICC) | <20 cm/s (southward) | 8-4° C | 34.5-34.8 psu | 400-1200 m |
| Upper Circumpolar Water (uCPW) | | | | | 1200-1500 m |
| North Atlantic Deep Water (NADW) | Deep Western Boundary Currents (DWBC) | Slow flow (~2 cm/s) (southward) | ~3° C | >34.8 psu | 1700-2000 m |

896

898 **LIST OF FIGURES CAPTIONS**

899 **TITLE:**

900 *MIDDLE TO LATE PLEISTOCENE PALAEOCEANOGRAPHY INFERRED*
901 *FROM RIDGE-FURROW STRUCTURES ON THE CONTINENTAL SLOPE*
902 *OFFSHORE ANGOLA*

903

904 Hugo Putuhena^{1*}

905 Andrew M.W. Newton²

906 Joe Cartwright³

907 Mads Huuse¹

908

909 **Manuscript submitted to:**

910 *Marine Geology – special issue*

911

912 * hugo.putuhena@manchester.ac.uk

913 *1) Department of Earth and Environmental Sciences, The University of Manchester, M13 9PL,*
914 *Manchester, United Kingdom*

915 *2) School of Natural and Built Environment, Queen's University Belfast, BT7 1NN, Belfast,*
916 *United Kingdom*

917 *3) Department of Earth Sciences, University of Oxford, OX1 3AN, Oxford, United Kingdom*

Fig.1. (a) Map of the sub-tropical section on the West Africa passive margin that shows the locations of published studies based on the analysis of 3D seismic data, including the site of this case study in (c). In each of the 3D seismic sites, there is an abundance of linear depression/furrow structures that have been identified. Insets (b, c, and f) show the outlines of the observed features in the Lower Congo Basin (b – Gay et al., 2004, 2006, 2007; c – This study, Jones et al., 2014; Jatiault et al., 2019; f – Maia et al., 2016), while (d) shows the outlines observed in the Gabon Basin (Lonergan et al., 2013), and (e) the outlines observed in the Kwanza Basin (Serié et al., 2017).

Fig.2. (a) Regional map showing the surface to deep thermohaline circulation in the modern-day South Atlantic Ocean, with water column stratigraphy shown profiles A08 (b), A10 (c), and A13 (d). Light blue dashed lines represent the three profiles. The water columns is comprised of the Surface Water (SW), Antarctic Intermediate Water (AAIW); upper Circumpolar Water (uCPW); North Atlantic Deep Water (NADW); and the Antarctic Bottom Water (AABW). The surface currents circulation was gathered from Hardman-Mountford, 2003 and Hopkins et al., 2013; AAIW, uCPW, and AABW circulation from Stremma and England, 1999; and NADW circulation from Arhan et al., 2003). The water mass profiles of A08 and A11 were gathered from Holfort and Siedler (2001) and the water mass profile of A13 were gathered from Arhan et al. (2003). The nomenclature of the water mass profile of A13 were matched to those in the A8 and A11 profiles. The background bathymetry and topography maps were obtained from ESRI.

Fig.3. (a) An example of ridge-furrow structure morphology on a combined dip and depth map of the seabed (SB) surface found in the study area – location of the inset can be seen in Fig.4.a. (b) is the superimposed (10:1 ratio toward the horizontal scale) seismic profile of the seismic stratigraphy on X-X' line located depicting the subsurface of the furrow structures and the presence of subtle intervening ridge structures among the furrows, while (c) is the line-drawing interpretation of the seismic stratigraphy in the interval of interest from the Top

Gelasian (TG) to the seabed (SB). The black solid vertical bars in (c) show the central furrows location in the cross-section, while the dashed black bars show the center line of the ridges.

Fig.4. Maps of ridge-furrow structure occurrence in the study area, which consist of (a) Map of dip and bathymetry of the seabed (SB) surface in the study area, depicting the presence of furrows and the distribution of furrow bifurcation points, (b) map of dip and bathymetry of the Cirq-1 (TG) surface in the study area showing the presence of the typical furrows across the area on that palaeo-surface. Black dotted lineaments in 3D view of (b) signs 10 ms TWT depth contour.

Fig.5. (a) Section of the seabed (SB) dip map in northern part of the West-Field showing areas where furrow fields exist. Cross-sections Y-Y' (b) and Z-Z' (c) show the subsurface of these areas. Location of the sections can be seen on Fig.4a. BSR is a bottom-simulating reflector observed across the study area.

Fig.6. Orientation and migration characteristic of the furrows in West-Field (a) and East-Field (b).

Fig.7. Spacing characteristic of the furrows in West-Field (a) and East-Field (b).

Fig.8. Sinuosity index (SI) and bifurcation occasion characteristic of the furrows in West-Field (a—sinuosity index, c—bifurcation occasion) and East-Field (b—sinuosity index, d—bifurcation occasion). The classification of the SI (almost straight, winding, twisty, and meandering) is based on the conventional classes of river sinuosity.

Fig.9. Section in the southern West-Field that shows the comparison between the outlines of furrow structure orientation on the seabed (SB) and the polygonal fault system plan-form pattern on the TG surface (a). The furrows outlined on the SB were based on the structure

(dip and depth) map (b), while the polygonal faults outline on the TG surface was based on the TG variance attribute map (c). Location of the section can be seen in Fig.4.a. Coloured dots across A-A' line used to sign intersections of a seabed furrow on A-A' line; each different colour indicates a different individual furrow—it does not represent the seabed depth.

Fig.10. Section of the West-Field that compares furrow structure orientation on the seabed (SB) and the horizontal pattern of the polygonal fault system on the TG surface (a). The furrows outlined on the SB were based on the structure (dip and depth) map (b), while the polygonal faults outline on the TG surface was based on the TG variance attribute map (c). Location of the section can be seen in Fig.4.a. Coloured dots across B-B' line used to sign intersections of a seabed furrow on B-B' line; each different colour indicates a different individual furrow—it does not represent the seabed depth.

Fig.11. Seismic profiles in (a) the southern West-Field section [A-A'] and (d) East-field section [B-B'] that depicts the presence of the furrow structures. Furrow occurrence on seismic profiles are described as convex downward depressions on the seismic reflections. The seismic profile also exhibits the dipping pattern of the Plio-Pleistocene polygonal faults system tier (from ~BP[Base Pleistocene] to TG[Top Gelasian]). The furrows presence on the seabed (SB) are depicted on the seismic profile as the coloured circles. The convex accent of furrows on the SB is depicted clearer on the seabed topography in c – for the [A-A'] profile and f – for the [B-B'] profile. The comparison of vertical dipping patterns of the stacked furrows and the polygonal faults system in the shallow interval is shown on the rose diagrams (b) – for the [A-A'] profile and (e) – for the [B-B'] profile. The rose diagrams display the vertical dipping patterns in cross-section plane, where the red colour depicts the dipping trend of the stacked furrows and the black depicts the dipping trend of the polygonal faults. Location of A-A' and B-B' can be seen in Fig.9a and 10a, respectively.

1000

1001 **Fig.12.** Maps depicting furrow migration behaviour through time captured in the southern West-
1002 Field section. (a) shows the outline map of the furrows on the seabed (SB) and TG compared
1003 to modern slope contours. The furrow outline for each surface was digitised from the structure
1004 map of dip and depth map such as given in the small inset in the section, (b) is the structure
1005 map on the seabed (SB) and (c) is on TG surface. The thickness in between the two surfaces
1006 in the inset is given in (d) and the contour of the thickness map is given in (e). Location of the
1007 section can be seen in Fig.4a. Coloured dots in each figure have same function with those in
1008 fig.9. In (e), red arrows represent observed furrows migration direction from TG to SB, purple
1009 contour lines represent 1 ms TWT contour of SG-TF thickness for thickness < the median
1010 value in (d), which is 60 ms TWT, and yellow contour lines represent 1 ms TWT contour of
1011 ST-TG thickness for thickness > the median value.

1012

1013 **Fig.13.** Maps depicting furrow migration behaviour through time captured in the East-Field
1014 section. (a) shows the outline map of the furrows on the seabed (SB) and TG surface
1015 compared to modern slope contours. The furrow outline for each surface was digitised from
1016 the structure map of dip and depth map such as given in the small inset in the section, (b) is
1017 the structure map on the seabed (SB) and (c) is on TG surface. The thickness in between the
1018 two surfaces in the inset is given in (d) and the contour of the thickness map is given in (e).
1019 Location of the section can be seen in Fig.4a. Coloured dots in each figure have same function
1020 with those in fig.9. Legend for (a) can be seen in Fig.11. In (e), red arrows represent observed
1021 furrows migration direction from TG to SB, purple contour lines represent 1 ms TWT contour
1022 of SG-TF thickness for thickness < the median value in (d), which is 70 ms TWT, and yellow
1023 contour lines represent 1 ms TWT contour of ST-TG thickness for thickness > the median
1024 value.

1025

1026 **Fig.14.** The conceptual model of the relationships of furrow structures orientation and
1027 migration observed in the study site versus all plausible near bottom flow directions that may

have generated the observed orientation and migration of the ridge-furrow structures based on known theoretical argument and observations of the furrows or sediment wave formation (Cartigny et al., 2011; Flood, 1988; McWave, 2017; Wynn and Stow, 2002). (a) depicts the inferred flow direction based on the conceptual model of the relationship between furrow orientation and migration in western furrow field and flow direction if the furrows are erosive features/longitudinal bedforms, which both would be parallel or lightly oblique upon each other (Hernández-Molina et al., 2011; Rebesco et al., 2014). While (b) is same with (a) but using the furrow migration and orientation in eastern furrow field (with a degree of curvature from the furrows aligning pattern). (c & e) depict the possible flow direction using the relationship between furrow orientation and migration in western furrow field and flow direction if the furrows are sediment waves generated by turbidity/density flow currents, where the furrows would be perpendicular to a flow direction. While (d & f) is using the furrow migration and orientation in eastern furrow field. (g, i, k & m) depict the possible flow directions using the relationship between furrow orientation and migration in western furrow field and flow direction if the furrows are sediment waves generated by bottom-currents, which the furrow orientation would be oblique $<45^\circ$. While (h, j, l, & n) using the furrow migration and orientation in eastern furrow field. The left table underneath the diagram exhibits whether (a-b) and (c-f) fulfil the conceptual criteria of erosive furrows and sediment waves generated by turbidity/density flow currents respectively as gathered from the related references (for erosive features: Flood, 1994; Hernández-Molina et al., 2008; Rebesco et al., 2014, for sediment waves generated by turbidity/density flow currents: Cartigny and Postma, 2017; Wynn and Stow, 2002). While the right table underneath the diagram exhibits whether (g-n) fulfil the conceptual criteria of sediment waves generated by bottom-currents as gathered from the related references (e.g., Cartigny et al., 2011; McCave, 2017; and Wynn and Stow, 2002). The circles display a traffic light system showing whether each model fulfils the conceptual criteria for sediment wave formation: i) meets the conceptual criteria and is contextually feasible (green), ii) meets the conceptual criteria but does not fit the study area oceanographic context (amber), and iii) does

not fulfill the conceptual criteria (red). Thus, conceptual models marked with a green signal are the most likely candidates for sediment wave formation.

Fig.15. Juxtaposition of the observed furrow structures (orientation and migration) towards the inferred bottom-current flows from different furrow definitions and origin assumptions, and the modern-day bottom current profile measured nearby. (a) The orientation direction of the observed furrows. (b) The migration direction of the observed furrows. (c) The inferred bottom-currents mean flow if the furrows were defined as erosional events. (d) The inferred bottom-currents mean flow if the furrows were defined as troughs of sediment wave formed by bottom-currents, to northwest. The inference is based on the common relationship of flow direction against sediment waves of bottom-currents bedforms (McCave, 2017; Wynn and Stow, 2002). (e) The inferred bottom-currents mean flow if the furrows defined as troughs of sediment wave formed by density flow, to southsouthwest. The inference is based on the common relationship of flow direction against sediment waves of turbidity-currents bedforms (McCave, 2017; Wynn and Stow, 2002). (f) The modern bottom-current profile from the 48 h measurement of mooring-station (1). (g) The modern bottom-current profile from the one year measurement of mooring station (2). The latter bottom-current profile shows the imprint of oscillating currents in the bottom-current regime in the region with the southward domination flow due to thermohaline currents (see oceanography background section for further explanation). To be noticed the bottom current profile may not represent the truly direction of the bottom-current regime in the study site, since the measurement located ~50 km to the southeast that may have different slope strike configuration to the study area.

Fig.16. Schematic model of all the bottom-current flows that are considered likely to become the origin of the ridge-furrow structures observed in the study site. The bottom-currents flow is either distal overflow of Congo Canyon (thin red arrows) (a), cascading of dense shelf water (thin purple arrows) (b) of the Angola Currents (AC) (thick purple arrows) or Benguela Coastal Currents (BCC) (dark blue arrow), or internal waves (light blue wavy arrow) (c), or a

1083 combination of them. The Congo Canyon overflow could be amplified by the addition of the
1084 cascading of dense shelf water (x) and sensitive to the variation of the climate and
1085 environmental conditions on the land, for example high precipitation may result in high river
1086 input and hence increase the turbidity flow intensity (y). The model is not to scale.
1087

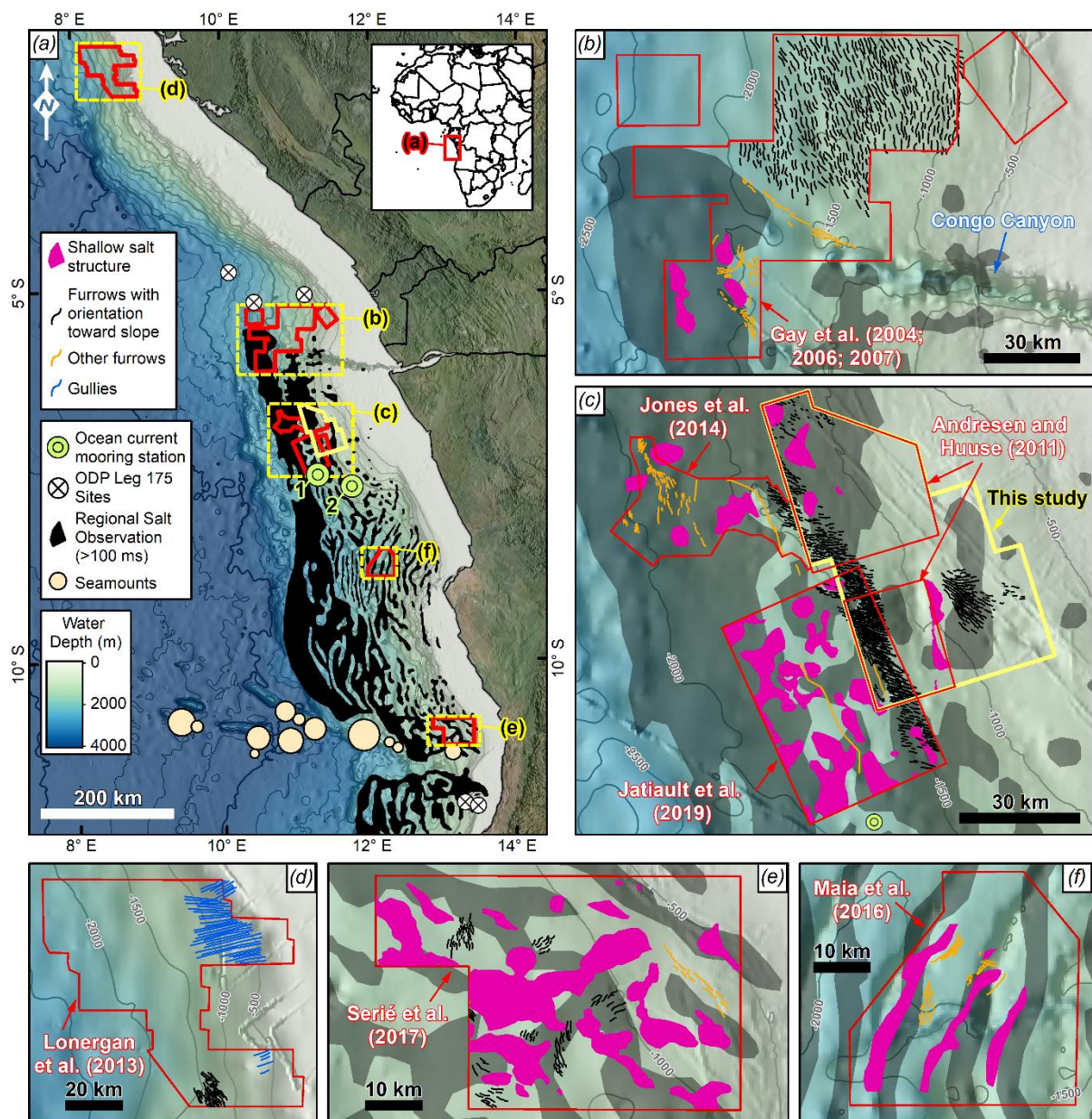


Fig.1

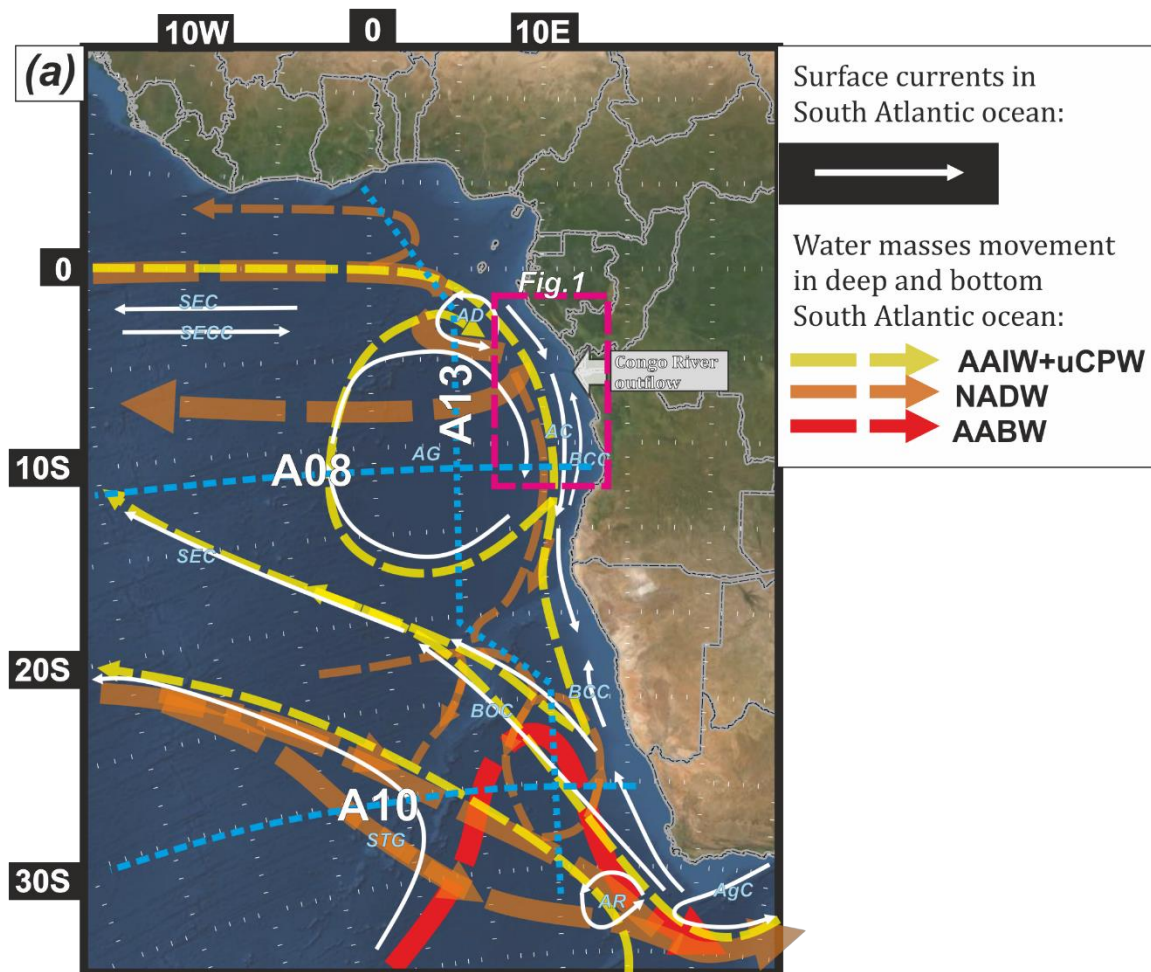


Fig.2(a)

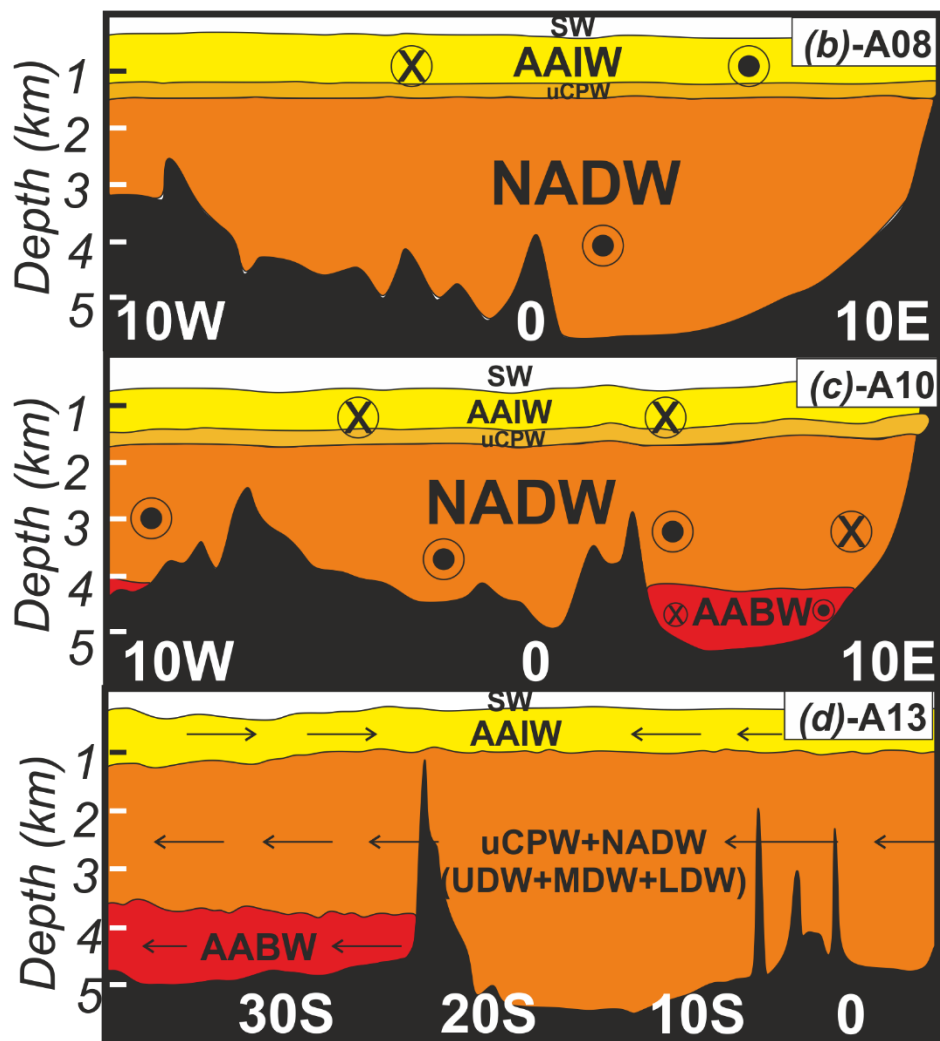


Fig.2(b-d)

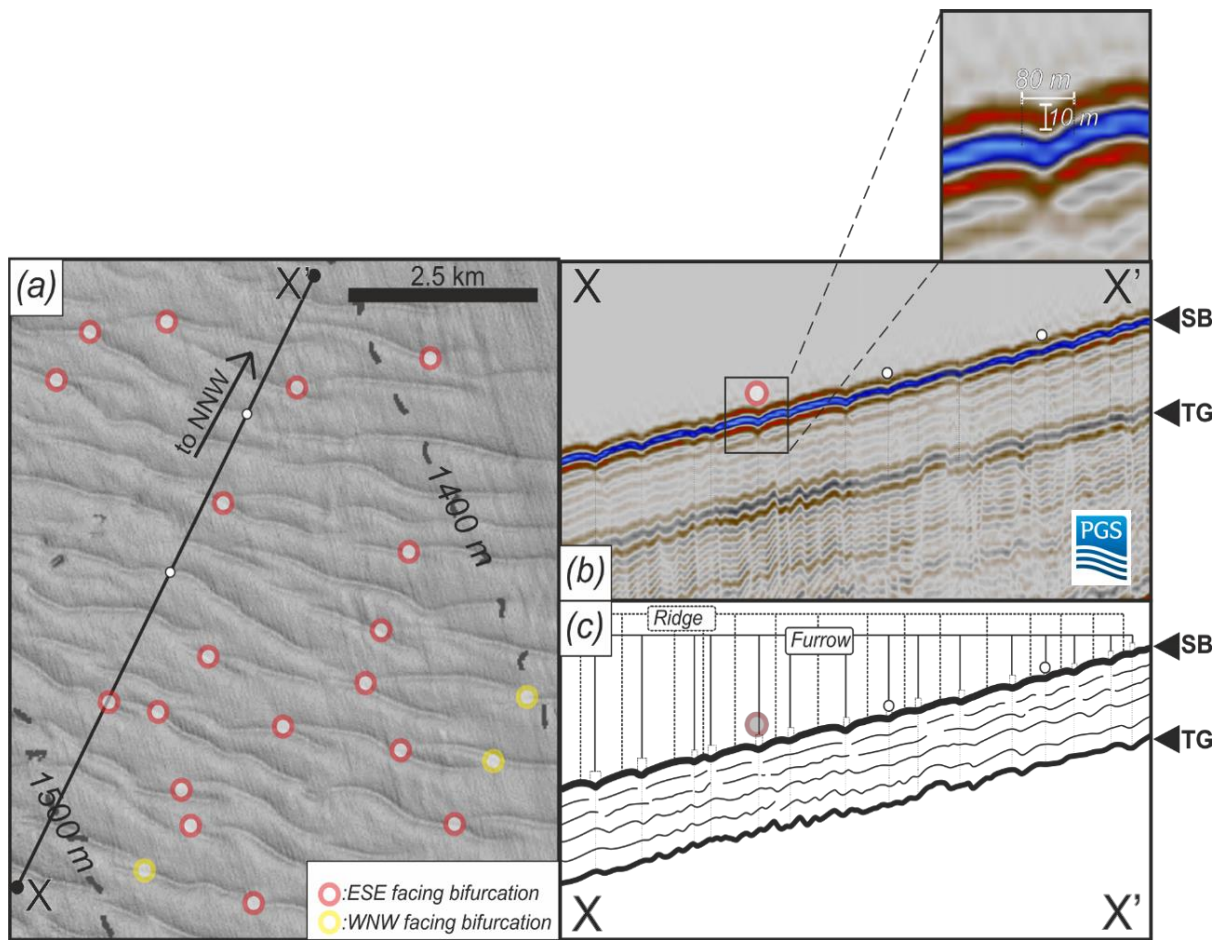
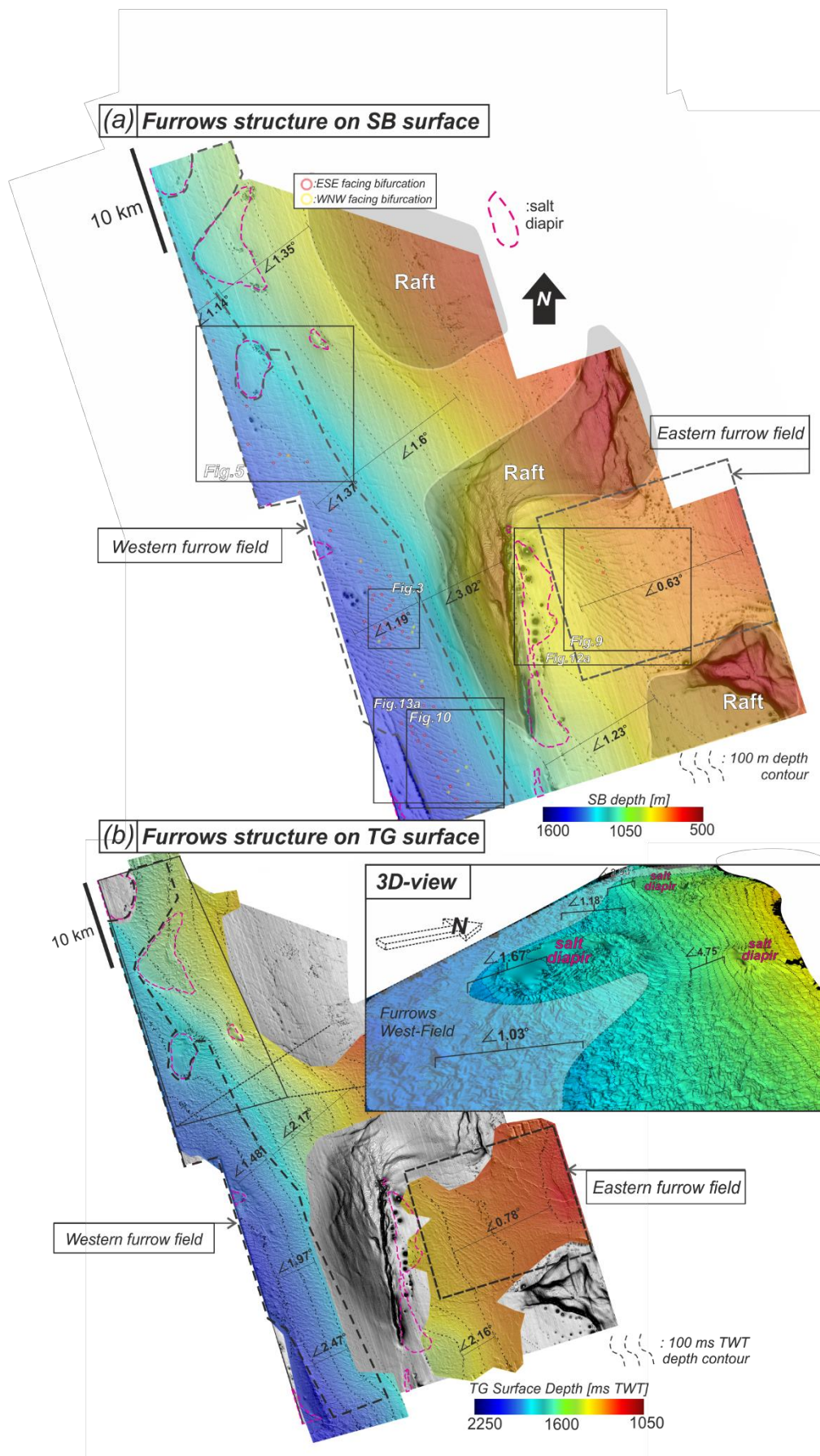


Fig.3



1100

1101 **Fig.4**

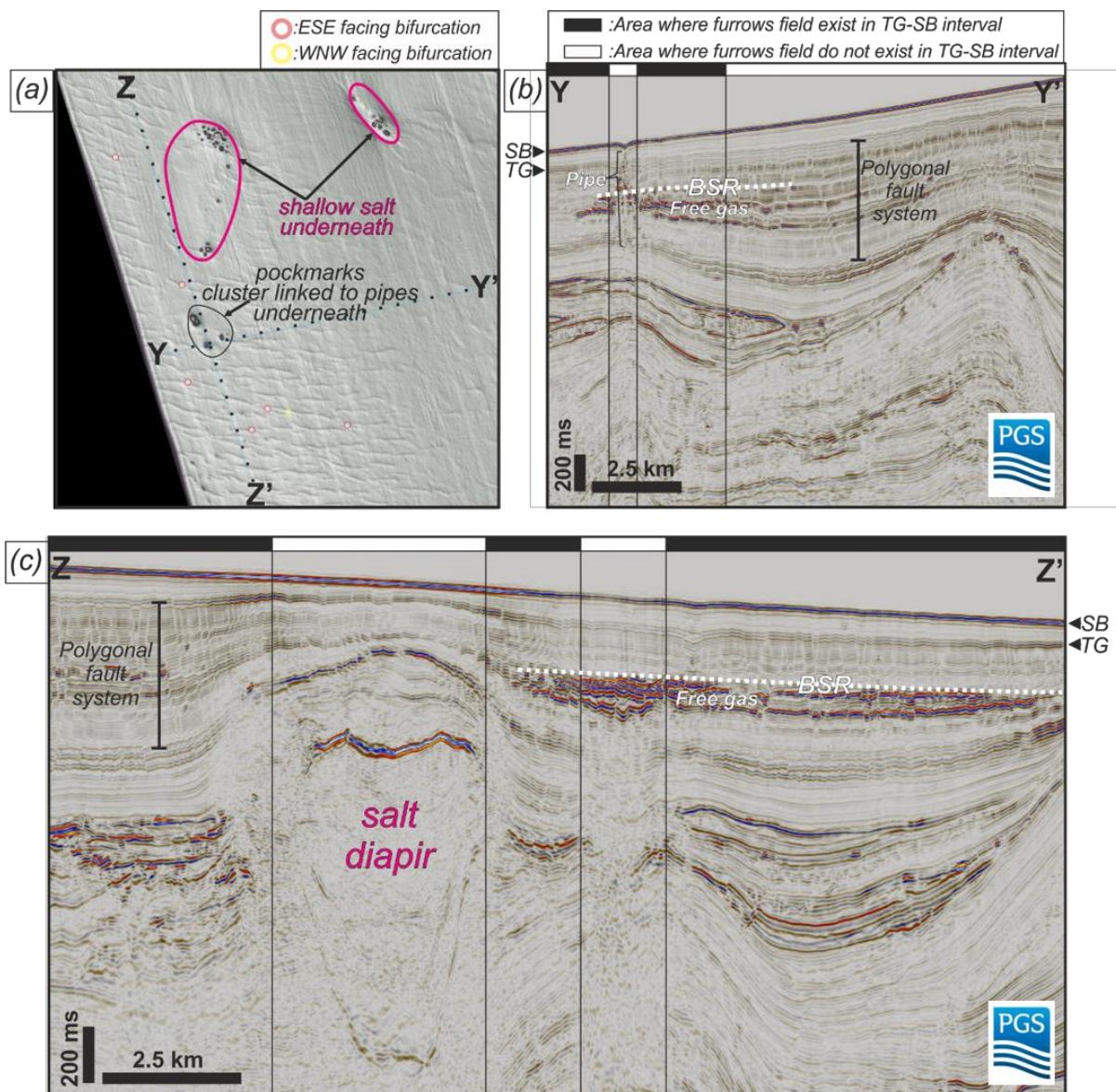


Fig.5

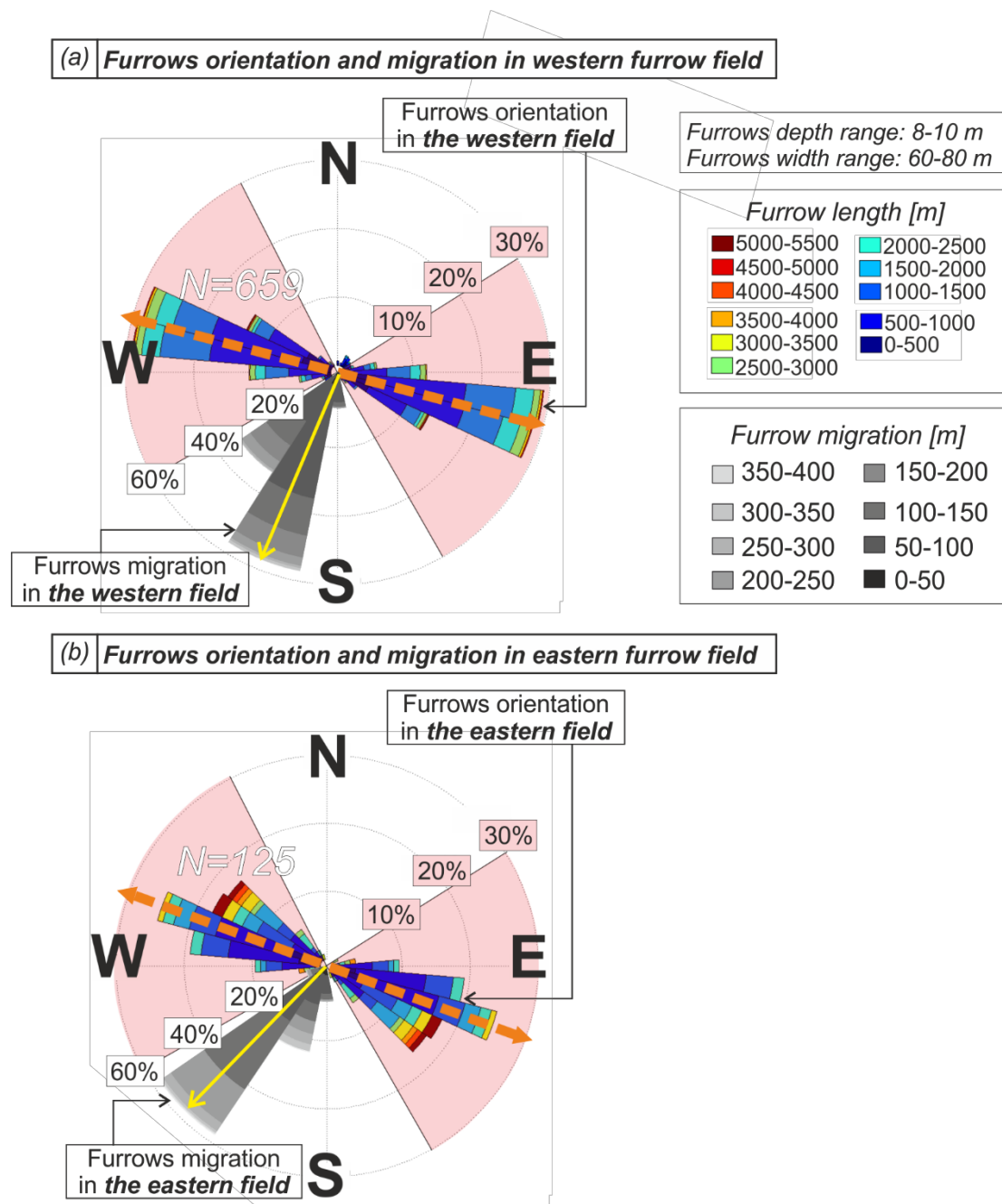
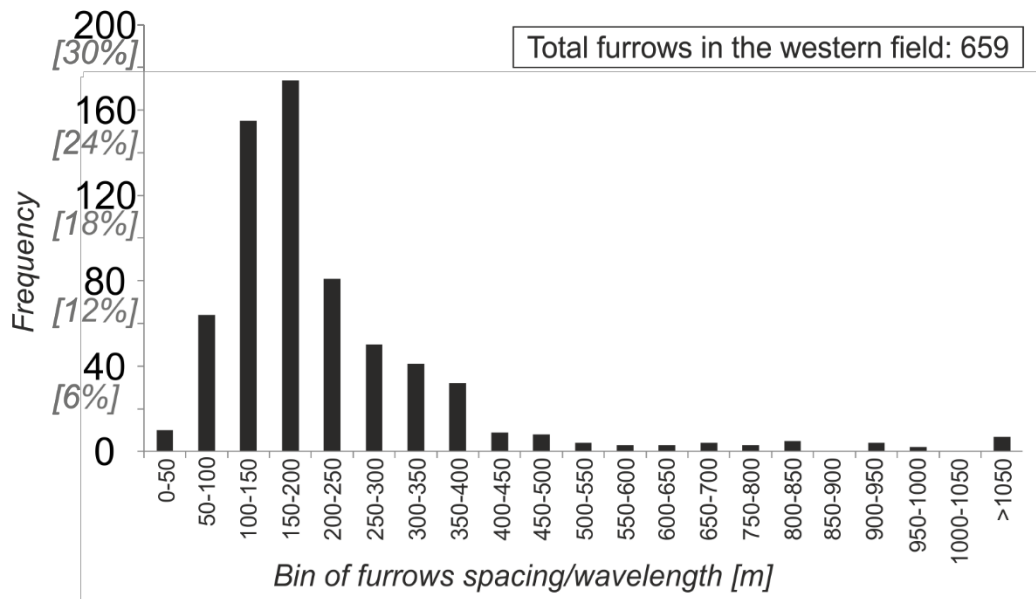


Fig.6

(a) *Furrows spacing in western furrow field*



(b) *Furrows spacing in eastern furrow field*

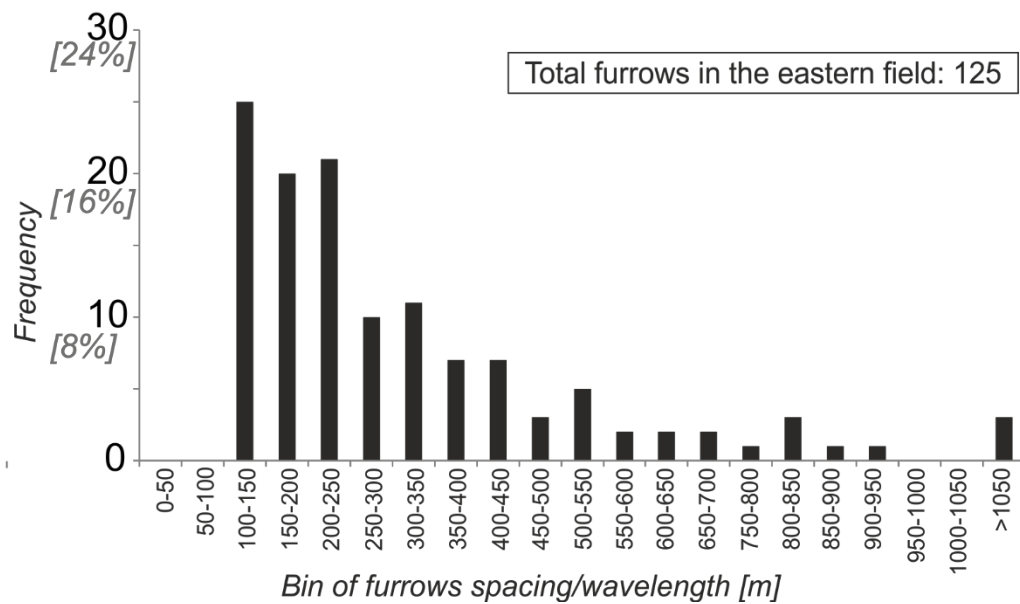
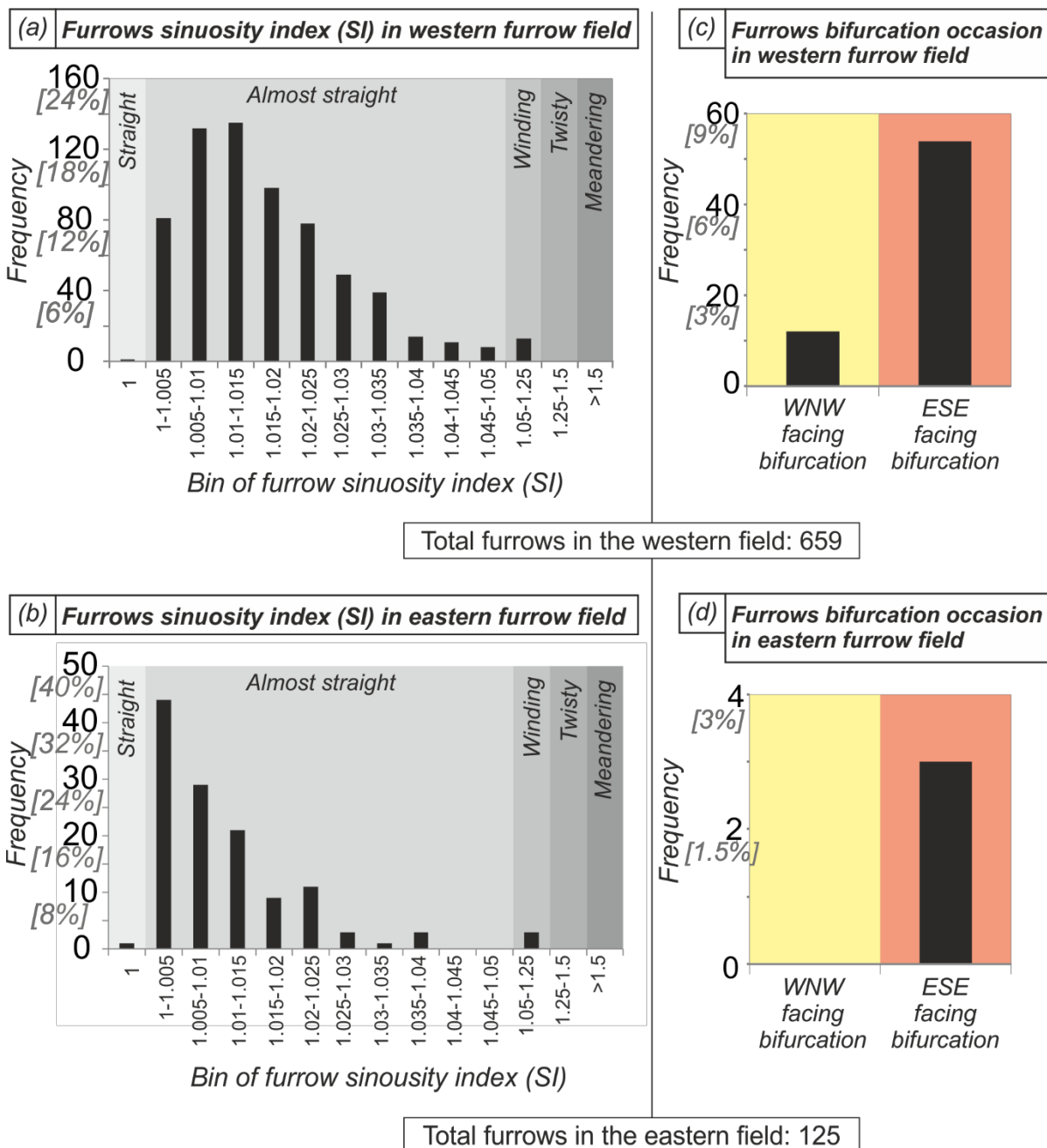


Fig.7



1111

1112 **Fig.8**

1113

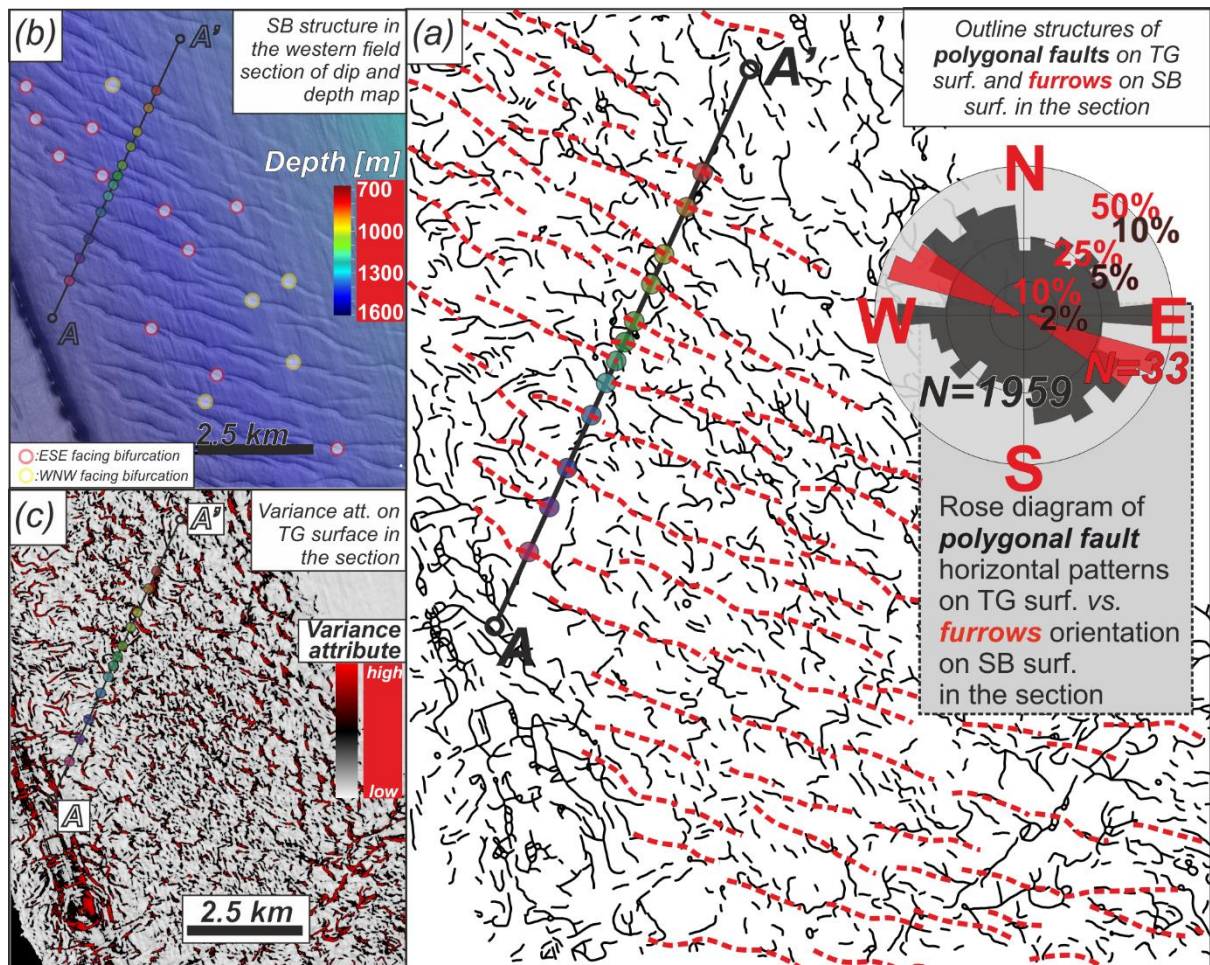


Fig.9

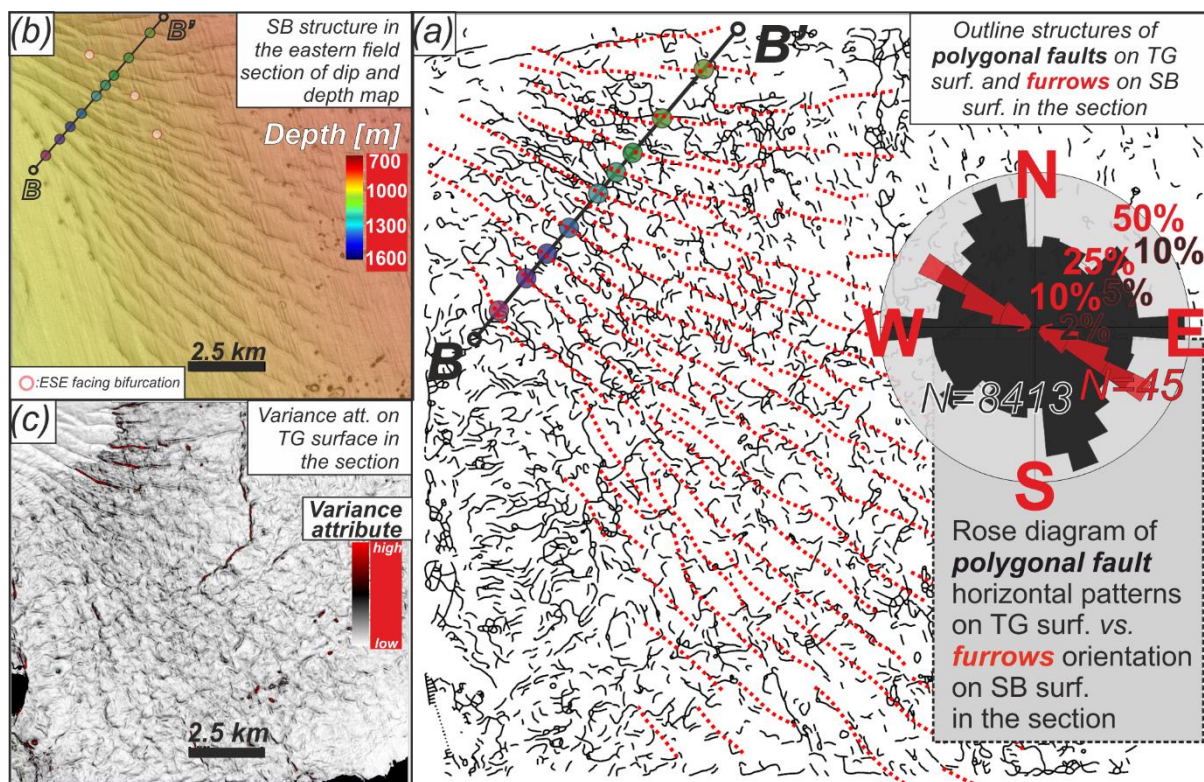
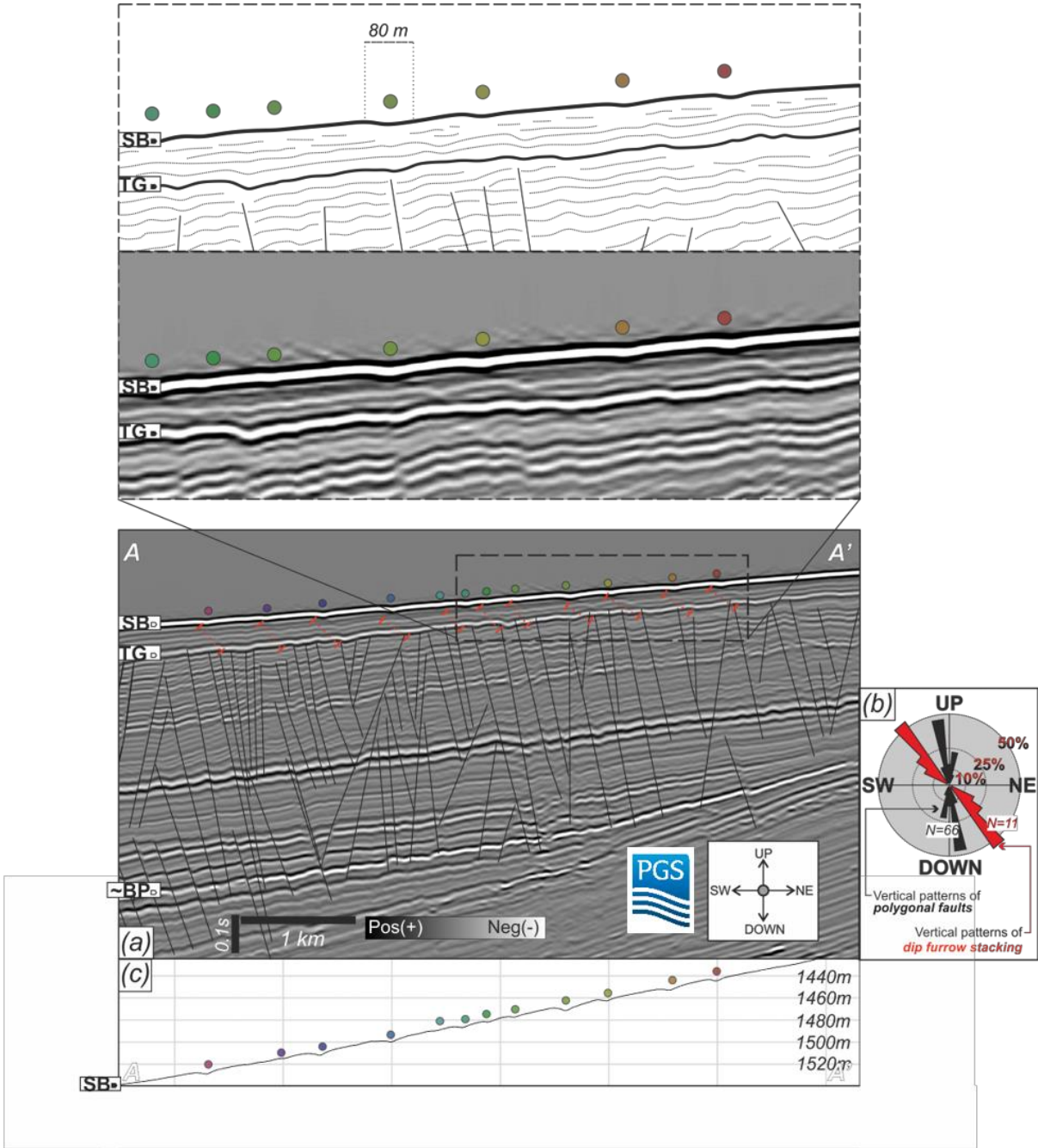


Fig.10



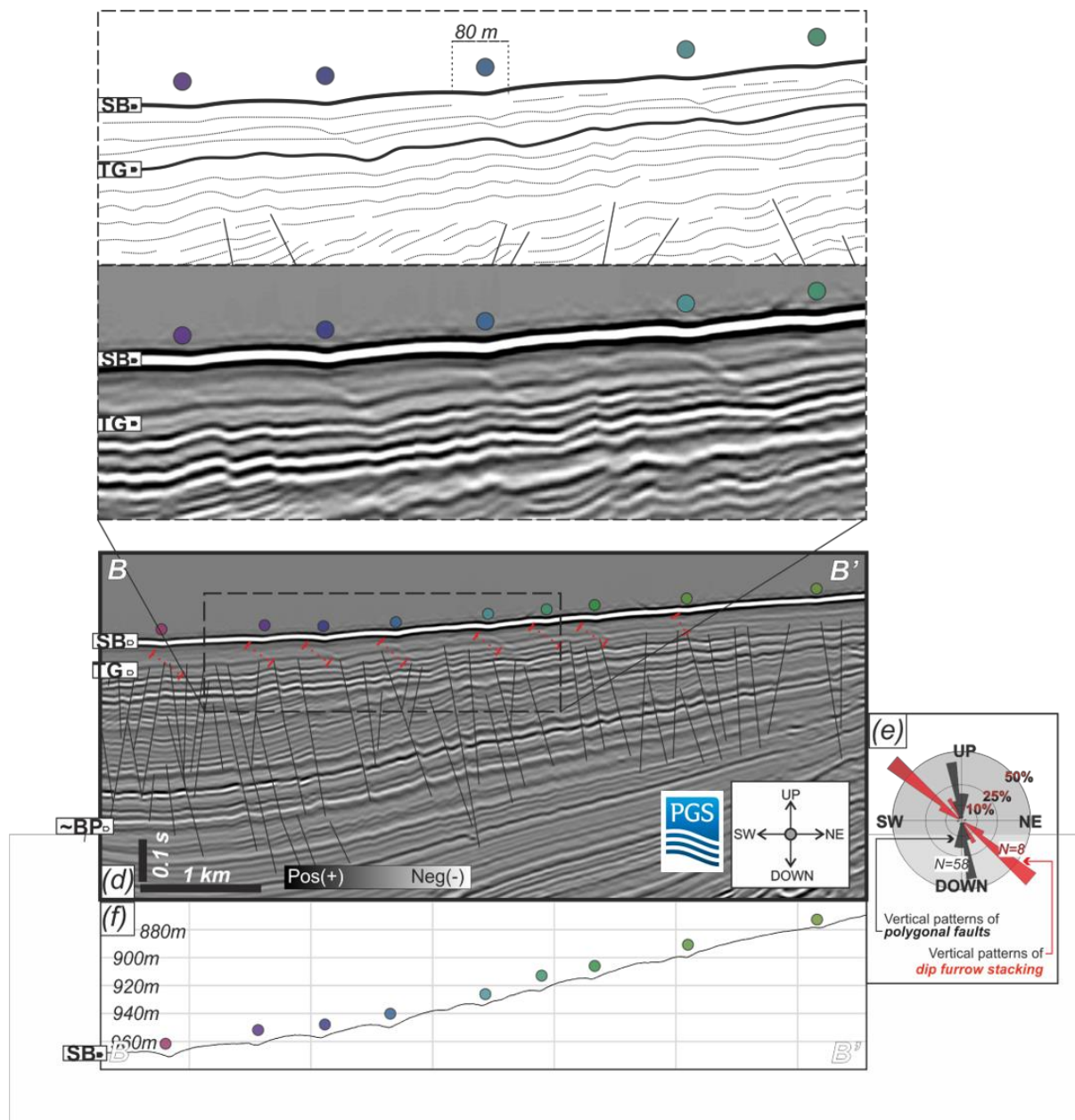


Fig.11(d-f)

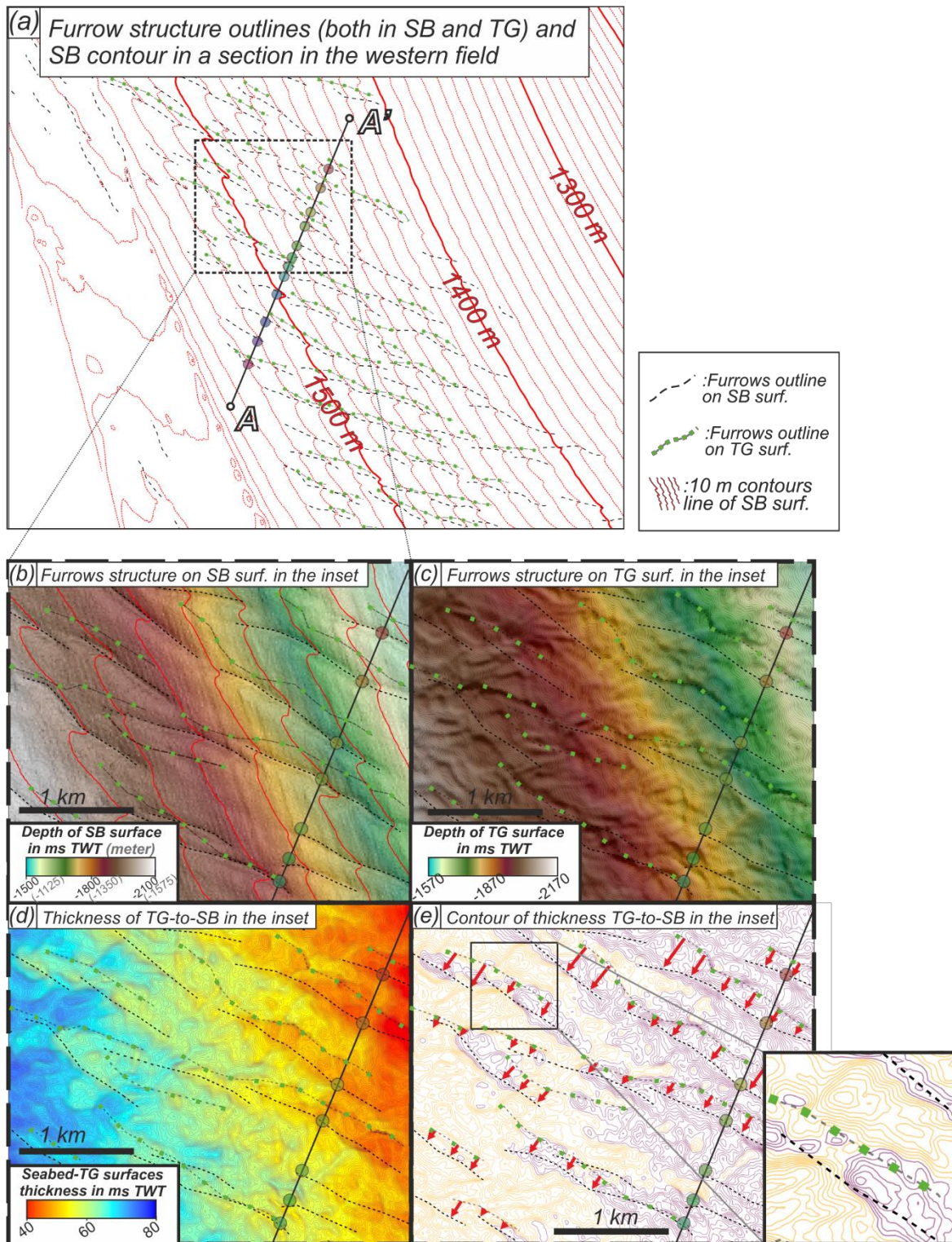


Fig.12

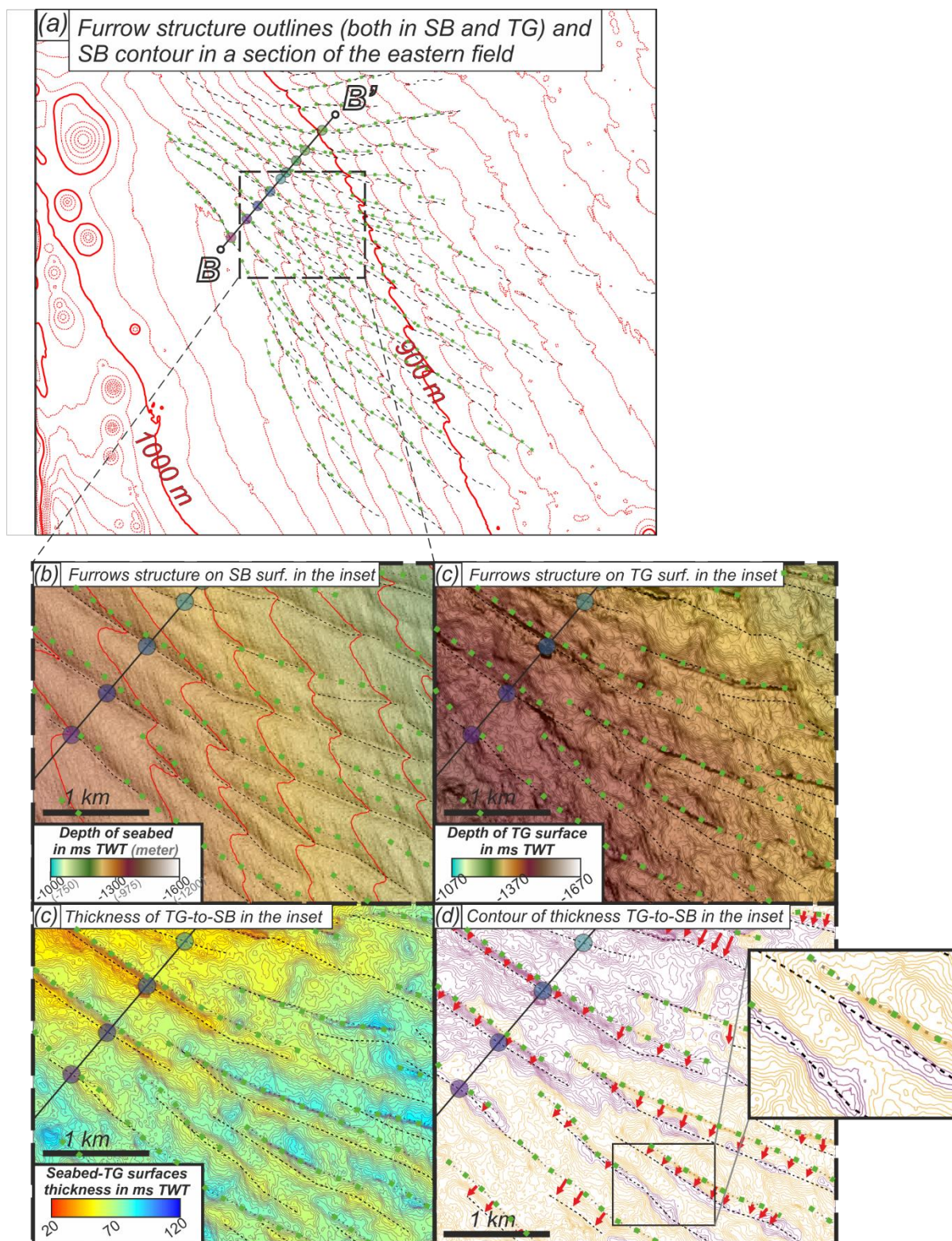
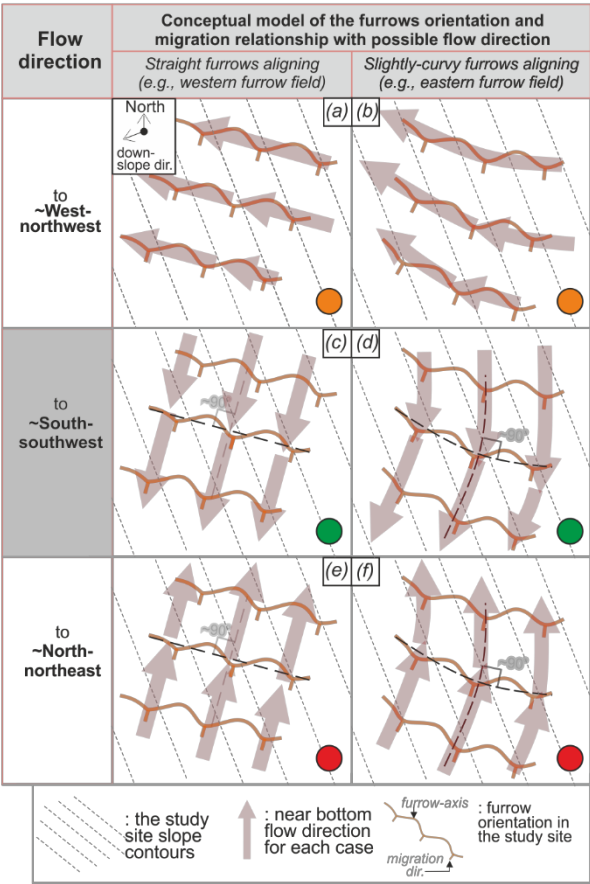
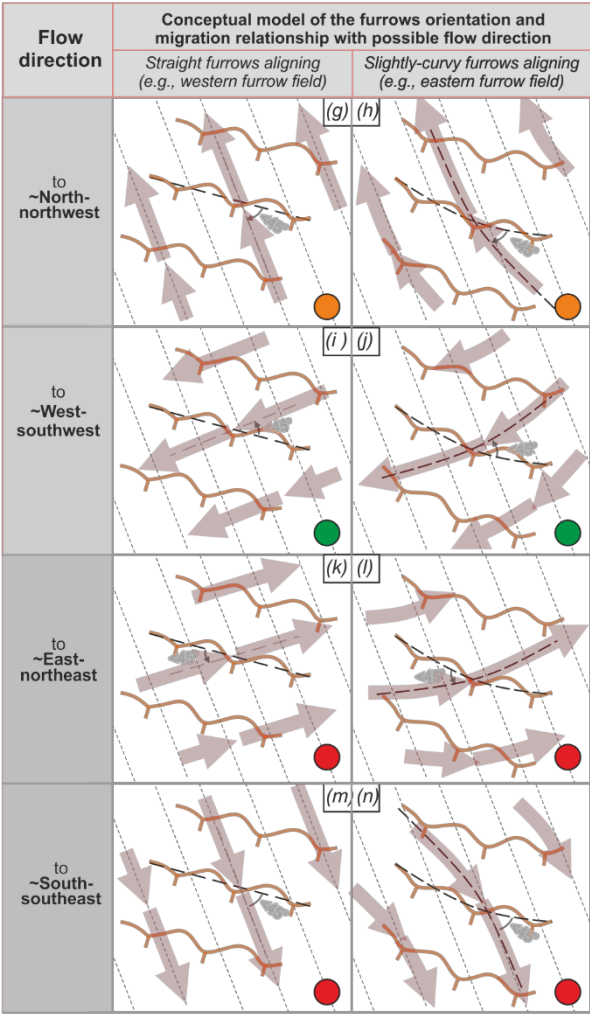


Fig.13



| Flow direction | Conceptual criteria of erosive furrows (Flood, 1994; Hernández-Molina et al., 2008; Rebesco et al., 2014) |
|------------------------------|-----------------------------------------------------------------------------------------------------------------------------------------------------------------------------------------------------------------------------------------------------------------------------------------------------------------------------------------|
| to ~West-northwest (a-b) | <input checked="" type="checkbox"/> Flow direction is parallel to the orientation of ridge-furrow longitudinal axes <input checked="" type="checkbox"/> Furrows migrating to the left of the flow direction |
| Flow direction | Conceptual criteria of turbidity-currents and their sediment waves (Cartigny and Postma, 2017; Wynn and Stow, 2002) |
| to ~South-southwest (c-d) | <input checked="" type="checkbox"/> Flow direction is perpendicular to the orientation of ridge-furrow longitudinal axes <input checked="" type="checkbox"/> Flow direction is in downslope/slightly downslope direction <input checked="" type="checkbox"/> Sediment waves could migrate downslope or upslope, or just aggrading |
| to ~North-northeast (e-f) | <input checked="" type="checkbox"/> Flow direction is perpendicular to the orientation of ridge-furrow longitudinal axes <input checked="" type="checkbox"/> Flow direction is in downslope/slightly downslope direction <input checked="" type="checkbox"/> Sediment waves could migrate downslope or upslope, or just aggrading |



| Flow direction | Criteria of bottom-currents and their sediment waves (Cartigny et al., 2011; McCave, 2017; Wynn and Stow, 2002) |
|------------------------------|--------------------------------------------------------------------------------------------------------------------------------------------------------------------------------------------------------------------------------------------------------------------------------------------------------------------------------|
| to ~North-northwest (g-h) | <input checked="" type="checkbox"/> Flow is steeply oblique (<45°) to the orientation of ridge-furrow longitudinal axes <input checked="" type="checkbox"/> Furrows migrating to the left of the flow direction <input checked="" type="checkbox"/> Sediment waves could migrate downslope or upslope, or just aggrading |
| to ~West-southwest (i-j) | <input checked="" type="checkbox"/> Flow is steeply oblique (<45°) to the orientation of ridge-furrow longitudinal axes <input checked="" type="checkbox"/> Furrows migrating to the left of the flow direction <input checked="" type="checkbox"/> Sediment waves could migrate downslope or upslope, or just aggrading |
| to ~East-northeast (k-l) | <input checked="" type="checkbox"/> Flow is steeply oblique (<45°) to the orientation of ridge-furrow longitudinal axes <input checked="" type="checkbox"/> Furrows migrating to the left of the flow direction <input checked="" type="checkbox"/> Sediment waves could migrate downslope or upslope, or just aggrading |
| to ~South-southeast (m-n) | <input checked="" type="checkbox"/> Flow is steeply oblique (<45°) to the orientation of ridge-furrow longitudinal axes <input checked="" type="checkbox"/> Furrows migrating to the left of the flow direction <input checked="" type="checkbox"/> Sediment waves could migrate downslope or upslope, or just aggrading |

Fig.14

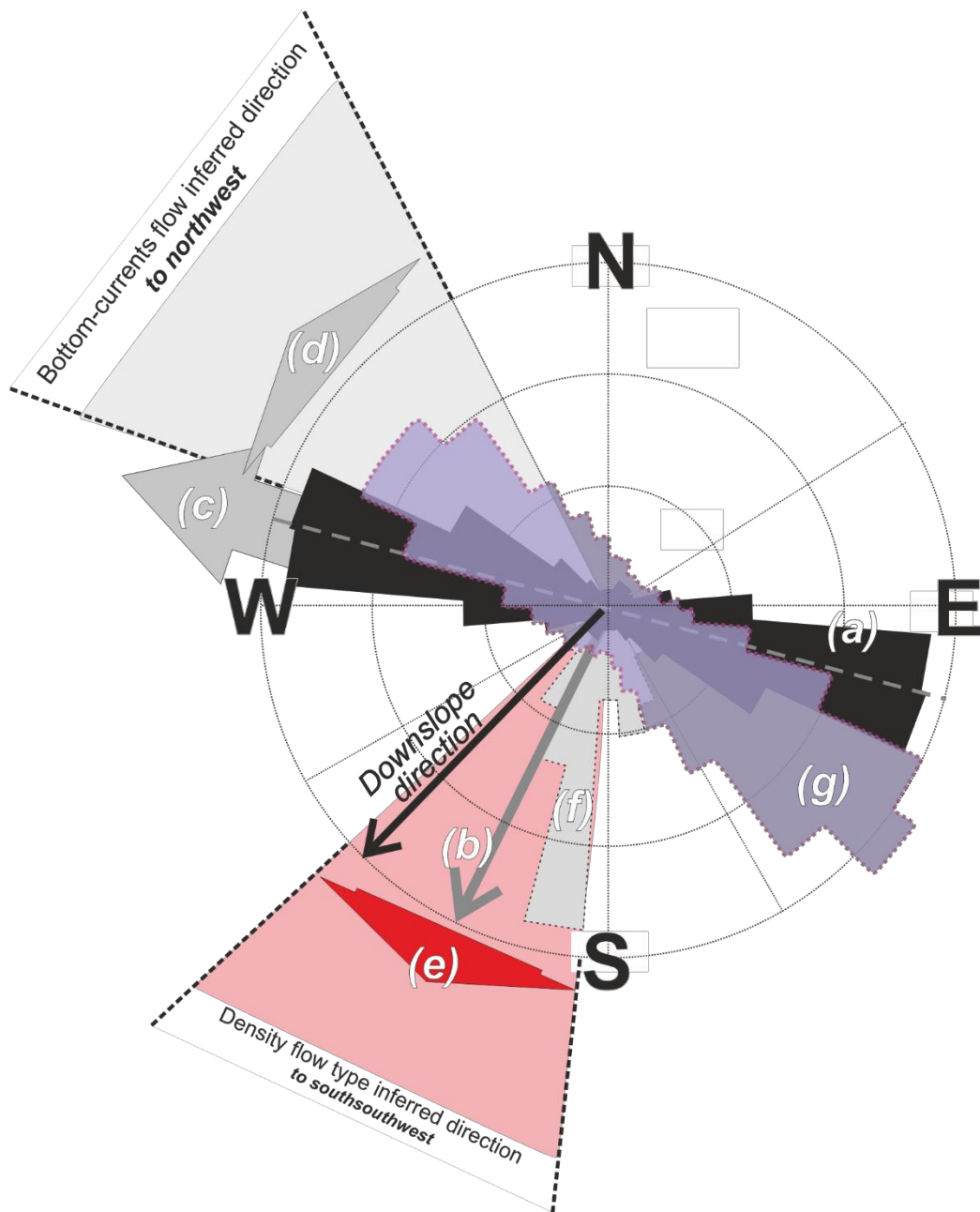


Fig.15

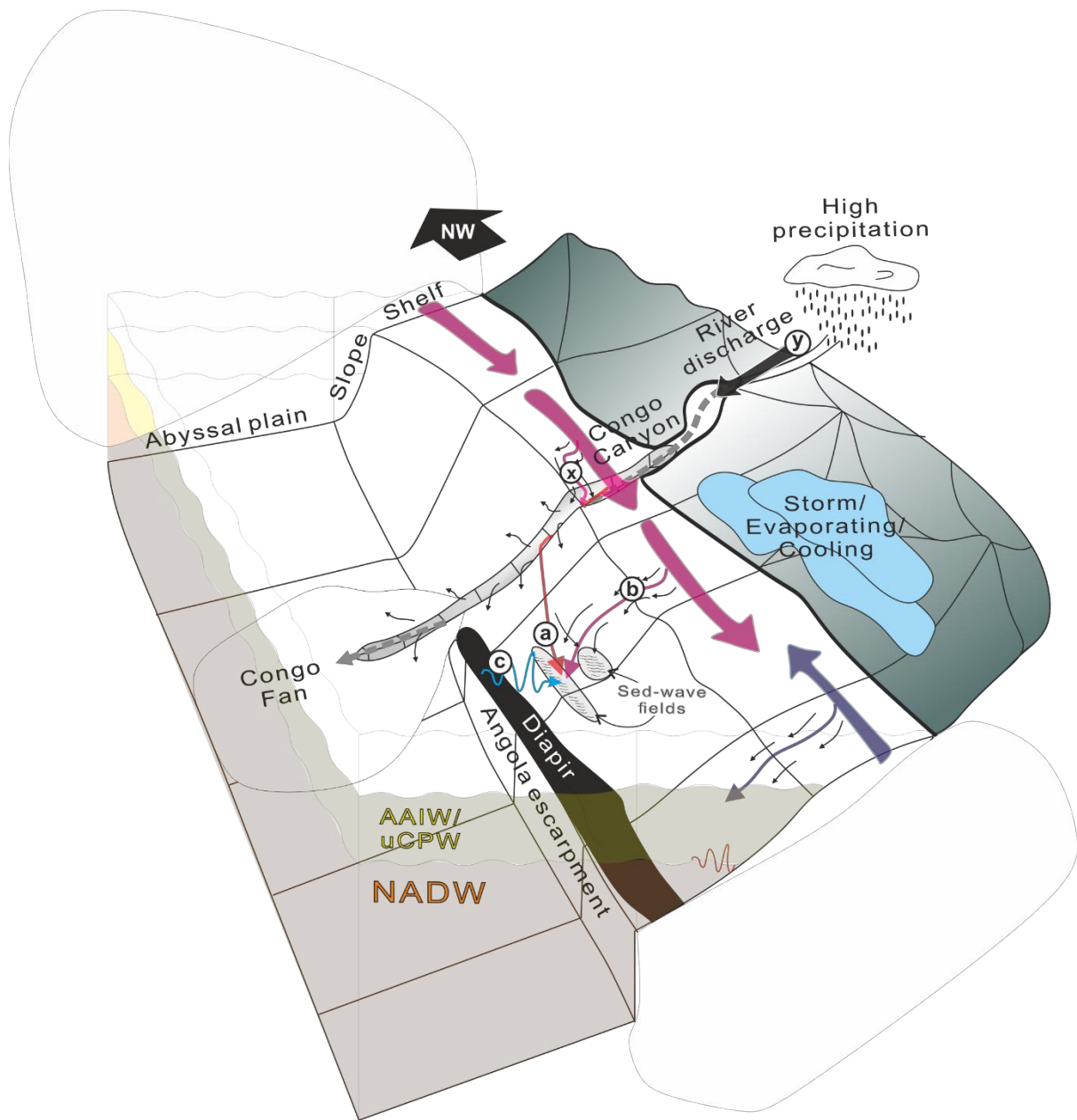


Fig.16